Review

Journal of RAMAN SPECTROSCOPY

Received: 15 March 2017 Revised: 6 September 2017 Accepted: 7 September 2017 Published online in Wiley Online Library

(wileyonlinelibrary.com) DOI 10.1002/jrs.5267

Unravelling external perturbation effects on the optical phonon response of graphene

Nedjma Bendiab,[a]* Julien Renard,[a] Cornelia Schwarz,[a] Antoine Reserbat-Plantey,[a,b] Léo Djevahirdjian,[a] Vincent Bouchiat,[a] Johann Coraux[a] and Laëtitia Marty[a]

Raman spectroscopy is a powerful and nondestructive probe that demonstrates its efficiency in revealing the physical properties of low-dimensional sp^2 carbon systems. It gives access to the number of layers, the quality and the nature of defects of all carbon allotropes, but also to the understanding of the influence of perturbations such as strain and/or doping. In this paper, we review the state of the art regarding the effect of external perturbations on the optical phonons of graphene. We describe how doping can tune the unusual electron–phonon coupling in graphene and thus modify not only the resonance conditions but also the phonon intensities thanks to quantum interferences. We also review the impact of strain on optical phonons and how one can disentangle strain and doping thanks to optical phonons. Last, implementations of this field to strain engineering or to graphene-based mechanical resonators will be presented. Copyright © 2018 John Wiley & Sons, Ltd.

Keywords: confocal Raman imaging; doping; strain; electron–phonon coupling; graphene

Introduction

Graphene is the first isolated 2D material; it has been extensively and efficiently studied by Raman spectroscopy, which turned out to be a powerful tool to unravel the graphene atomic structure and electronic properties. Its nondestructive character in addition to its high spectral resolution and the possibility of spatial imaging makes it reliable to extract the number of layers and the crystalline quality but also the doping level and the strain field. Despite the small number of Raman active modes in graphene, the interpretation of their wavenumbers, widths and intensities provides reliable information on graphene properties. The purpose of this review is to provide the background to understand how graphene optical phonons are modified under external perturbation like doping, strain or interaction with the substrate. In the first section, we will focus on the electron–phonon coupling effect in graphene and how tuning this coupling (by either doping or grafting) modifies the Raman spectra. Therefore, one can use this Raman fingerprint to extract the doping level and/or the strength of electron–phonon coupling in graphene. The second section will be dedicated to the effect of uniaxial and biaxial strain on graphene optical phonons. Finally, we will discuss how recent works allow us to disentangle strain and doping in the same graphene sample and how it could be extended to image strain field at a microscopic scale.

Effect of electron–phonon and/or exciton–phonon on the Raman response of graphene

Low-dimensional sp^2 carbon systems show a strong coupling between their electronic and their vibrational properties. The existence of a strong electron–phonon coupling in graphene is responsible for many of its most interestingphysical properties, for example, the possibility to tune its vibrational and electronic properties by an external electrostatic gate. Thus, the Raman spectra of such systems have to be analyzed by taking into account the electronic properties of the probed system. The electron–phonon coupling is also a fundamental issue to understand the electronic transport in such a system.

First of all, this part will briefly describe the Raman active modesin graphene that will be examined in detail thereafter. Because graphene has two atoms per unit cell, six normal modes (two being doubly degenerate) at the center of the Brillouin zone are possible[1]: A_{2u}, B_{2g}, E_{1u}, E_{2g}. There is only one degenerate in-plane optical mode, E_{2g}, and one out-of-plane optical mode B_{2g}. The E_{2g} phonons are Raman active, whereas the B_{2g} phonon is neither Raman nor infrared active.[2] The Raman spectrum of monolayer graphene consists of different bands, which can be interpreted by inspecting the optical phonon dispersion[3] (Fig. 1). The high wavenumber peak named G peak corresponds to the E_{2g} phonon at 1580 cm^{-1}. The D peak is due to the breathing modes of the six-atom rings (Fig. 1) and requires a defect for its activation.[4–6] It comes from transverse optical (TO) phonons at the K points of the Brillouin zone.[4–6] The D mode is active in a double-resonance process and is strongly dispersive with excitation energy, owing to a singularity at the K point.[80] Double resonance can also happen as an intra-valley process, that is, connecting two points belonging to the same cone around K (or K′). This gives rise to the so-called D′ peak. The 2D peak is the D peak overtone, and the

* *Correspondence to: Nedjma Bendiab, Univ. Grenoble Alpes, CNRS, Grenoble INP, Institut Néel, 38000 Grenoble, France. E-mail: nedjma.bendiab@neel.cnrs.fr*

a *Univ. Grenoble Alpes, CNRS, Grenoble INP, Institut Néel, 38000 Grenoble, France*

b *ICFO-Institut de Ciencies Fotoniques, The Barcelona Insitute of Science and Technology, 08860 Castelldefels, Barcelona, Spain*

Journal of RAMAN SPECTROSCOPY

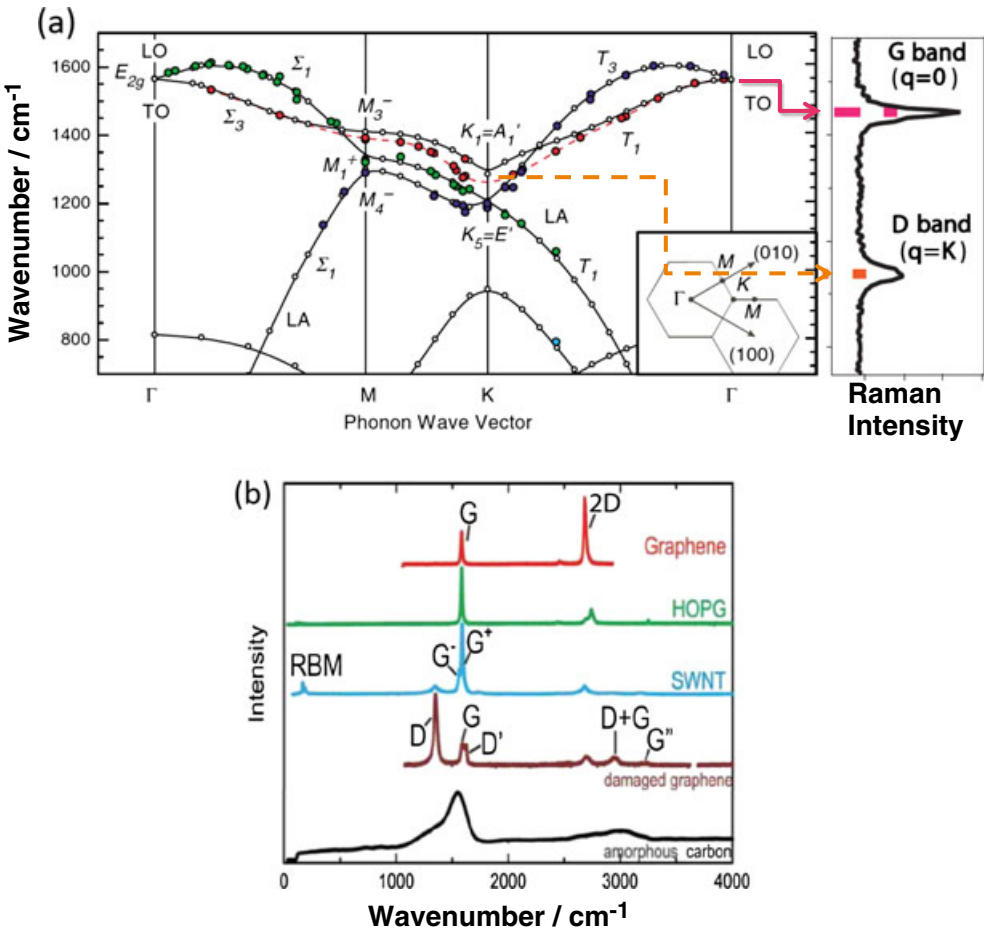

Figure 1. Raman modes of graphene. (a) Phonon dispersion of graphite from Maultzsch *et al.* in regard with Raman spectrum of graphene. Adapted with author permission from Maultzsch *et al.*[3] Copyright 2004 American Physical Society. (b) Typical Raman spectra of graphite, graphene, damaged graphene and nanotubes by Dresselhaus *et al.* Reprinted with permission from Dresselhaus *et al.*[146] Copyright 2010 American Chemical Society. HOPG, highly oriented pyrolytic graphite; RBM, radial breathing mode; SWNT, single-walled carbon nanotube.

2D′ peak is the D′ overtone. Because the 2D and 2D′ peaks originate from a Raman process where momentum conservation is satisfied by two phonons with opposite wave vectors, no defects are required for their activation, and these peaks are thus always present in the Raman spectra.

In this section, we will discuss electron–phonon coupling in graphene and recent advances in its understanding. Graphene is a π-conjugated one-atom-thick 2D membrane. As a consequence, its electronic structure is highly sensitive to its environment, which allows external charges (from absorbed molecules or under application of an external field) to be easily transferred to it. This sensitivity to charges enables to tune the electronic properties, in field effect transistors with dielectric[7] or ionic[7,20,21] gating, or with the help of intercalation[14] and for instance to control proximity-induced superconductivity.[8] Charge carrier densities of the order of few 10^{12} cm-2 are reached with solid back-gates,[11] while higher values are accessible with ionic gating. Moreover, the variation of the charge density in graphene strongly influences its optical phonons owing to the strong electron–phonon coupling.[7,9–19] By tuning charge transfer in such an sp^2 carbon system, we can modulate this coupling and obtain a full picture of its origin and mechanism.

Effect of doping on first-order Raman mode

In graphene and also in nanotubes (Fig. 2), the shift of the Fermi level induces an unusual phonon stiffening of the G phonon and also a narrowing of its width, which indicates a modification of its lifetime. These phenomena are related to the presence of singularities at the Γ point and at K and K′ (referred to as Kohn anomalies in the literature), which results in a strong electron–phonon coupling as discussed in several works.[16,22,23,25,26] Thus, the strong electron–phonon coupling affects significantly the dependency of the phonon wavenumber with charge transfer. This dependency can be used to determine precisely the position of the Dirac point in the case of the anomaly at the K point. Although somehow imprecise, the use of the term Kohn anomaly to refer to these phonon anomalies is widely spread in the literature. Regarding the G phonon intensity dependency with the Fermi level, the role of the different available quantum pathways is crucial and will be discussed later.[27–29] Finally, recently, a Fano resonance was observed on monolayer graphene at the charge neutrality point, and its dependency with the Fermi level was discussed by Hasdeo *et al.*[29,31]

More precisely, it has been observed that a shift in the Fermi level induces a hardening of the G mode for graphene and the corresponding LO (G^-) mode for nanotubes (Fig. 2). In the classical picture of the effect of charge transfer on optical phonons, we rather expect a softening of the mode if the graphene turns

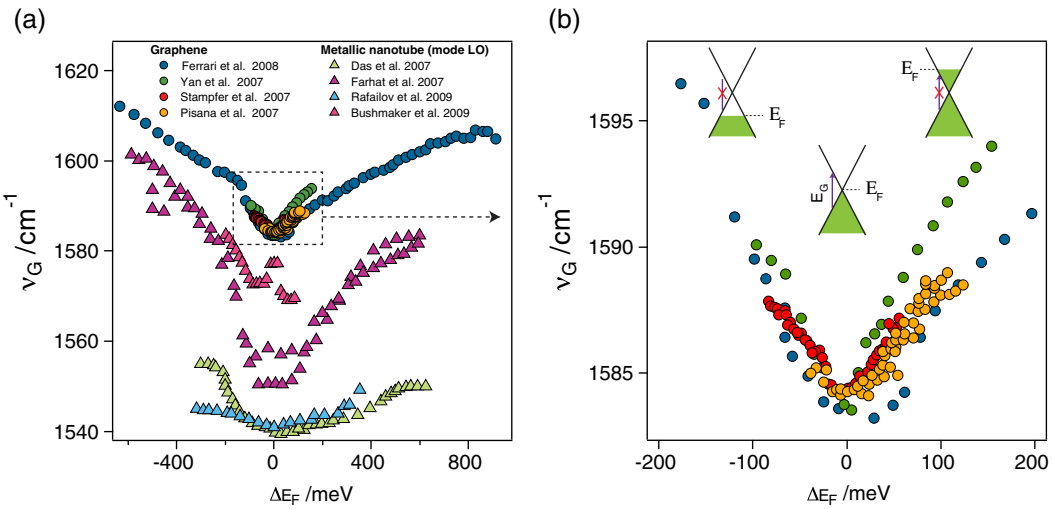

Figure 2. G mode dependency with electrostatic doping. (a) G mode wavenumber as a function of the Fermi level ($\Delta E_F = 0$ correspond to the Dirac point) for graphene and metallic nanotubes [longitudinal optical (LO) phonon]. (b) Zoom for the graphene at a low doping level. All the different data are derived from references (order of appearance in the legend)[7,9,10,12,13,17–19]

n-doped because it softens the force constant of the oscillator, whereas in the p-doped case, we expect the opposite behavior. In the case of graphene or nanotubes, whatever the doping (n-type or p-type), we always observe a hardening of the G mode. Moreover, the mode width takes its maximum value at the Dirac point and decreases for both doping types. These observations were finally explained thanks to a model developed by Caudal *et al.*[16] for single-walled carbon nanotubes and by Ando *et al.*[32] and Pisana *et al.*[19] for graphene. The dynamic matrix presents an electron–phonon coupling term that involves (1) an interband interaction (electronic transition between valence and conduction bands) and (2) an intraband interaction (an electronic transition within the same band). For a low amount of doping ($\Delta E_F <$ highest band), the interband electronic transitions dominate (this transition is represented with a cartoon in Fig. 2). By tuning the Fermi level close to the Dirac point, we pass from a regime of allowed transition to a regime where the transition is forbidden; energy conservation allows this change to occur when the Fermi level is shifted by an amount equal to half of the energy of the involved phonon: $\Delta E_F = E_{ph}/2 \sim 100$ meV. The transition probability vanishes only when $\Delta E_F = E_{ph}/2$ at $T = 0$ K. At finite temperature, the probability falls as does the density of available electronic states. The phonon spectrum has a singularity in the dispersion of the G mode at $q = 0$. This singularity is also observed for the modes (D and 2D) at $q = K$. Here we must emphasize that to properly describe these singularities (called Kohn anomalies), it is mandatory to consider the dynamics of the ions with respect to electrons. In fact, the Born–Oppenheimer approximation is no more valid at these Kohn anomalies. Thus, we must describe the energy variation $\Delta\nu_G$ of the G phonon at $q = 0$ as a function of the displacement u_i associated with this mode and the variation of the Fermi level $\Delta E_F(u)$, which depends on the positions of the ions because we are out of the Born–Oppenheimer approximation:

$$\Delta\nu_G = \frac{1}{2m\nu_G^0}\frac{d^2\Delta E_F(u)}{du^2} \quad (1)$$

An important consequence of this result is that during the atomic movement corresponding to the G mode, the disturbance of the electronic structure associated with this movement does not relax fast enough.[19] Regarding the G linewidth, we observe a decrease of the full width at half maximum and then a saturation.[11,33] This saturation occurs when the doping causes a shift of the Fermi level by a value equal or superior to the incoming photon energy. Actually, because of the Pauli principle, the phonon decay channel into electron–hole pairs is blocked. This means that the phonon lifetime increases when the Fermi level moves away from the Dirac point.

The case of second-order Raman modes

Regarding the 2D mode, the situation is controversial. The early work of Das *et al.*[11] reports a nonlinear wavenumber dependency of the 2D mode with the gate voltage roughly explained by their density functional theory calculations. However, recent works[33–35] show that the 2D line wavenumber and width behave the opposite way compared to the first-order G phonon (Fig. 3). The theoretical work of Hasdeo *et al.*[29,31] tries to solve this debate. In this work, the authors show that there is a competition between the intraband and interband excitations leading to a phonon renormalization dominated by the intraband electron–hole excitation over the Kohn anomaly effect. Thus, they conclude that the 2D mode behaves in the opposite way compared to the G mode regarding its wavenumber and linewidth.

However, the experimental work carried out by Liu *et al.*[40] on graphene on hexagonal boron nitride (h-BN; whereas previous works[11,34,35] were all focused on graphene on SiO_2) shows that the 2D mode wavenumber behaves similar to the G mode wavenumber, whereas its linewidth behaves in an opposite way. This discrepancy between graphene on SiO_2 and graphene on h-BN regarding the 2D wavenumber dependency with gate voltage allows them to conclude that the 2D mode dependency with the Fermi level points to electron–electron interactions that were not taken into account by Hasdeo *et al.*[29,31] even if it was earlier mentioned by Basko *et al.* as a possibility.[27]

Another important point is the variation of the phonon intensities with the Fermi level. In fact, all the works[11,34–36] show that first-order and second-order phonon modes exhibit different Raman intensity dependencies with the Fermi level. Moreover, inside the second-order family, the 2D mode does not behave as the other phonons. In an early work, Das *et al.*[11] showed a strong dependency of the intensity ratio I_{2D}/I_G with gate voltage.

Journal of RAMAN SPECTROSCOPY

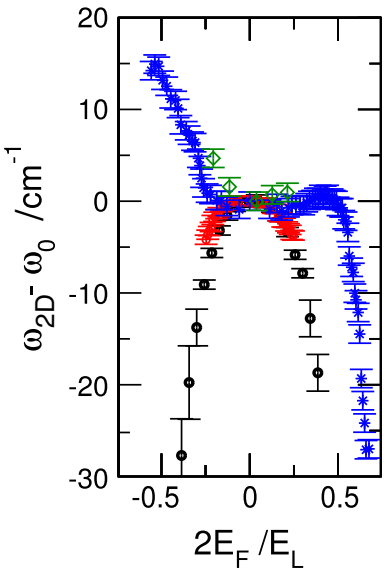

Figure 3. Evolution of the 2D mode wavenumber as a function of $2E_F/E_L$. Black dots correspond to Hasdeo calculations. Adapted with author permission from Hasdeo *et al.*[29] Copyright 2016 American Physical Society. The other data are experimental results (blue asterisks are from Das *et al.*,[11] red dots are from Araujo *et al.*[35] and green diamonds are from Yan *et al.*[17]). Discrepancies between the different experimental data are important because of a competition between the intraband and interband excitations that can be governed by electron–electron interactions, which differs from one work to another.

This dependency (for $E_F < 0.5$ eV) has been explained later on by Basko *et al.*[27] as due to electron–electron interactions that play an important role on the 2D mode intensity, whereas the G mode intensity for $E_F < 1$ eV is almost constant with doping.[27] The work of Chen *et al.*[28] shows that the G band intensity can be strongly enhanced depending on the Fermi level. In fact, they show that some of the G mode Raman pathways can be blocked by tuning the Fermi level. In that specific case, the G phonon Raman intensity increases dramatically. This increase is the expression of quantum interferences between the different Raman scattering pathways. This mechanism has been recently calculated by Hasdeo *et al.*[29] and by Reichardt *et al.*,[37] showing that the opposite phases between the incident resonance and the scattered resonance yield destructive interferences that are suppressed when the Fermi energy is close to half the laser energy. In fact, at this condition, as mentioned by Chen *et al.*, the scattered resonance cannot occur in agreement with the Pauli exclusion principle, thus, the G mode intensity increases.[28] Regarding the 2D mode intensity, the same work shows that a monotonic decrease occurs as the resonant Raman pathways become blocked. Hasdeo *et al.* show that the 2D mode does not show such destructive interference owing to the real character of the two electron–phonon matrix elements only in this specific case, whereas all other two-phonon combination modes present this destructive interference and thus have their intensities also enhanced for $E_F = 2E_L$.[28,29]

The case of the D mode

Because the D mode is usually used to determine the defect concentration by measuring the I_D/I_G ratio,[38,39] it is important to understand how this ratio depends on doping. It has been demonstrated by Liu *et al.*[40] that the characteristics of the D mode peak strongly depends on carrier density: (1) its wavenumber increases for hole doping and decreases for electron doping, (2) its linewidth broadens as the electron doping increases and sharpens as the hole doping increases, (3) its intensity is strongly enhanced when the energy of the intermediate state $E_k = E_L - \hbar\omega/2$ because of quantum interferences between the different Raman pathways and (4) its Raman intensity is higher for electron doping than for hole doping because of a stronger electron–phonon coupling for electron doping. The strong dependency of the D band and the G band with carrier density has to be considered when the ratio is used to characterize the quantity of defects in graphene samples. In a later work, Bruna *et al.* describe the dependency of the I_D/I_G ratio with the charge carrier density and present a general relation between D peak intensity and defect density, valid for any doping level.[41]

To summarize, we show that it is possible to gain insights on the doping level of a graphene sample by measuring its Raman spectrum. We note that, in the case of nanotubes, a lively discussion has been questioning for a decade the excitonic *versus* electronic origin of the coupling to phonons. Of course, in the case of nanotubes, the semiconductor nature of the tubes naturally raises the question. However, even if at first sight a zero-bandgap semi-metal such as graphene is not expected to show excitonic effects, it is interesting to consider this possibility over the whole Brillouin zone.

Exciton–phonon effect on the Raman response of graphene

The gapless electronic band structure of graphene does not straightforwardly point to strong excitonic effects with visible light, which is the usual range for Raman spectroscopy (Fig. 4). This general statement can be confirmed by studying the absorption (transmission) of a graphene flake. One can observe that the spectrum is relatively featureless in the visible range,[42,43] especially for undoped graphene. Nevertheless, an excitonic feature can be seen in the near-ultraviolet range around 5 eV (Fig. 4).

It is related to transitions at the M point of the electronic band structure. The presence of this saddle point can have strong consequences on the Raman spectrum, especially on the second-order 2D mode. For excitation above the saddle point transition energy, that is 5 eV, some double-resonance processes are forbidden and the intensity of the peak is quenched, while the line shape is deeply changed.[44–46] Interestingly, the energy position of the saddle point can be tuned in twisted bilayer graphene. It depends on the respective alignment of the two layers.[47,48] The resonance energy can then be brought in the visible range for some twisting angles. For instance, with a laser excitation at 633 nm (1.96 eV), the resonance is obtained for a misalignment of about 10°.[49] The intensity of the G peak is strongly enhanced when the resonance condition is met (Fig. 5).

This section shows the importance of electron–phonon coupling in low-dimensional sp^2 systems. The huge sensitivity to the environment thanks to electron–phonon coupling can be used for the detection of molecules or adsorbents for example (see the review paper of Kalbac and co-workers in this special issue). Moreover, any perturbation of the electronic structure of graphene translates in its optical phonons because phonons and electrons in such a low-dimensional material interact strongly. Finally, it is important to underline that a similar doping effect on the optical phonons and on photoluminescence has been reported recently on transition metal dichalcogenides,[50–53] indicating a more universal behavior of all the 2D materials.

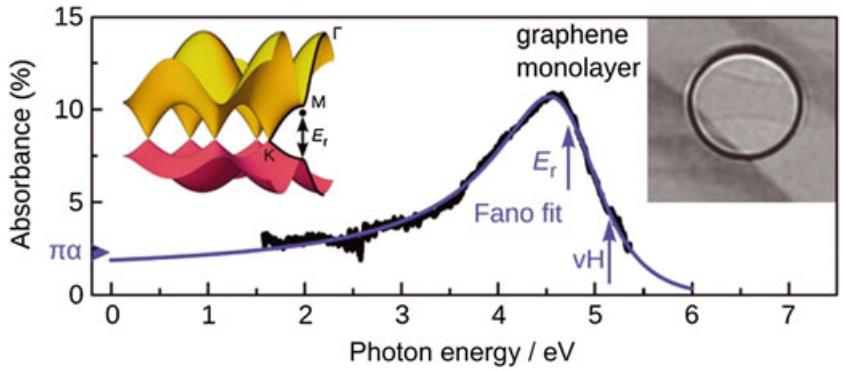

Figure 4. Optical absorbance of a free-standing graphene monolayer. While constant to $\pi * \alpha$ in a wide range around the visible, a strong resonance caused by the presence of a Van Hove singularity at the M point of the band structure is seen. Reprinted with permission from Chae *et al.*[42] Copyright 2011 American Chemical Society.

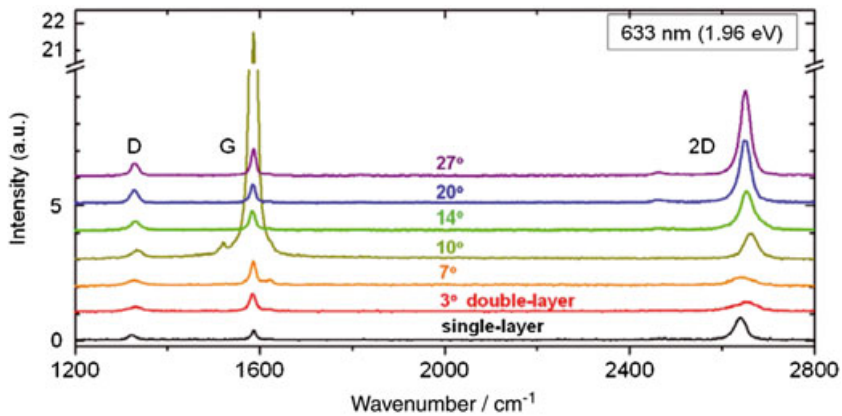

Figure 5. Raman spectra upon excitation at 633nm of single layer graphene and of twisted bilayer graphene. When the twist angle is at resonance (here ~10°), the G peak intensity is strongly enhanced. Reprinted with permission from Kim *et al.*[49] Copyright 2012 American Physical Society.

In the following section, we will describe how a mechanical effect, namely, a stress, can also modify the Raman fingerprint of graphene by deforming the atomic bonds or by changing the resonant Raman condition, which are directly linked to its electronic structure.

Effect of mechanical stress on the Raman response of graphene

The mechanical properties of a crystal are linked to the strength and stiffness of its interatomic bonds. Because graphene is an sp^2 carbon system, interatomic bonds are strong and stiff, endowing graphene with the highest in-plane Young's modulus found in material science. Its atomic structure combined with long-range π-conjugation gives not only superior mechanical properties but also non-common vibrational ones. Because bond length changes under deformation, the effective spring constant between the atoms hardens under compression and softens under tension, inducing at least a wavenumber shift of its optical phonons. Thus, by measuring the optical phonon modification under stress, one can access mechanical properties.

Three types of studies are present in the literature; the first one consists of applying a uniaxial stress on a polymer where the graphene is deposited as depicted on Fig. 6. The second one consists in applying biaxial stress by using a membrane of suspended graphene (Fig. 6b). A third kind of studies address the role of heteroepitaxial stress, between graphene and its substrate. In this section, we will mainly focus on the first two types of studies.

The case of uniaxial stress

In most cases, in order to ensure the controllability and the reproducibility of uniaxial stress experiments, the graphene monolayer is deposited on flexible substrates (mostly polymers), and the stress is applied on two-point or four-point bending experiments (Fig. 6). Typically, the size of the graphene layer is orders of magnitude smaller than the substrate length.[54,55] Cycles of loading and unloading are performed in order to check for reproducibility. The measurement of the G and 2D modes by Raman spectroscopy is then realized for each cycle. Experimentally (Table 1), the G mode dependency shows the same trend for all substrates because the deformation always changes the force constant between the atoms and thus the wavenumber of the Raman modes. Some early works on diamond and silicon show a similar behavior.[56–58] A possible origin of the observed variability is slippage of graphene onto the soft substrate, which is expected to mainly occur at high stress values (e.g. high values of the soft substrate deformation). In the presence of uniaxial stress, the dynamic equation for a phonon mode is

Journal of RAMAN SPECTROSCOPY

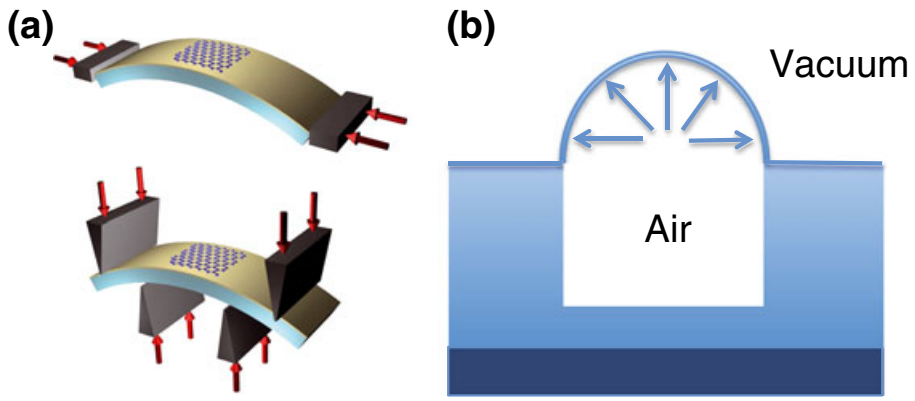

Figure 6. Applying stress on graphene. (a) Two-point and four-point bending methods to apply uniaxial stress on graphene. Reprinted with permission from Mohiuddin *et al.*[54] Copyright 2009 American Physical Society. (b) Blisters as a method to access biaxial strain on graphene (illustration of the method used by Zabel *et al.*[85]).

Table 1. Shift rates of G and 2D modes for uniaxial stress applied on different substrates

Graphene substrate	$\partial\omega_{G^+}/\partial\epsilon$ ($cm^{-1}/\%$)	$\partial\omega_{G^-}/\partial\epsilon$ ($cm^{-1}/\%$)	$\partial\omega_{2D}/\partial\epsilon$ ($cm^{-1}/\%$)	Strain details	λ (nm)	Comments	References
PET	−14.2	N/A	−27.8	Uniaxial $\in [0, 0.8\%]$	532	No G splitting	Ni *et al.*[60]
PDMS	−5.6	−12.5	−21	Uniaxial $\in [0, 3.5\%]$	532	G splitting at 0%	Huang *et al.*[59]
PET	−10.8	−31.7	−64	Uniaxial $\in [0, 1.3\%]$	514.5	G splitting for $\epsilon > 0.1\%$	Mohiuddin *et al.*[54]
PMMA	−17.5	−36	N/A	Uniaxial $\in [0, 0.7\%]$	785	G splitting for $\epsilon > 0.05\%$	Frank *et al.*[55]
PMMA	−14.5	−33.4	N/A	Uniaxial $\in [0, 0.7\%]$	514.5	G splitting for $\epsilon > 0.05\%$	Yoon *et al.*[61]

N/A, not applicable; PDMS, polydimethylsiloxane; PET, polyethylene terephthalate; PMMA, poly(methyl methacrylate).

$$-m\ddot{u}_i = \overbrace{m\left(\nu^0\right)^2 u_i}^{\text{without stress}} + \overbrace{\sum_{klm} K_{iklm}\epsilon_l m u_k}^{\text{with stress}} \quad (2)$$

with m the mass of ions, $u_{i=x,y,z}$ the movement of ions along the directions in space and ν^0 the phonon mode wavenumber without strain ($\epsilon = 0$). The second term describes the change induced by strain ϵ. K_{iklm} is an element of the force constant tensor K. Solving Eqn 2 mainly consists of solving the secular equation leading to the values of ν, roots of the dynamic equation (see for graphene the works of Huang *et al.*[54,55,59]). In the case of graphene, applying a uniaxial stress leads to two eigenmodes for the G band, called ν_{G+} and ν_{G-} and defined as

$$\begin{cases} \nu_{G+} = \nu_G^0 - \mathcal{A}^+\epsilon \\ \nu_{G-} = \nu_G^0 - \mathcal{A}^-\epsilon \end{cases} \quad (3)$$

with $\mathcal{A}^+$ and $\mathcal{A}^-$ two functions depending on the graphene Poisson coefficient (which is taken as the in-plane graphite one, about $\nu = 0.13$).[54] For uniaxial stress applied, a longitudinal strain $\epsilon_L = \epsilon$ occurs, but also another strain appears along the perpendicular direction $\epsilon_T = -\nu\epsilon$. These two terms form the hydrostatic strain $\epsilon_h = \epsilon_L + \epsilon_T$ and the shear strain $\epsilon_s = \epsilon_L - \epsilon_T$. The Grüneisen coefficient γ and the shear coefficient β for the doubly degenerate mode E_{2g} (the G band) are related to these two types of strain induced by a uniaxial stress[54]:

$$\begin{cases} \gamma = -\frac{1}{\nu_G^0}\frac{\partial\nu_G^h}{\partial\epsilon_h} \\ \beta = -\frac{1}{\nu_G^0}\frac{\partial\nu_G^s}{\partial\epsilon_s} \end{cases} \quad (4)$$

The overall dependency of the G mode wavenumber with strain has been experimentally demonstrated by several groups (Fig. 7). The G mode softens with strain and degeneracy is lifted at high strain values.

In Fig. 7, we can see that the expected linear dependency between the G mode wavenumber and the strain occurs only for

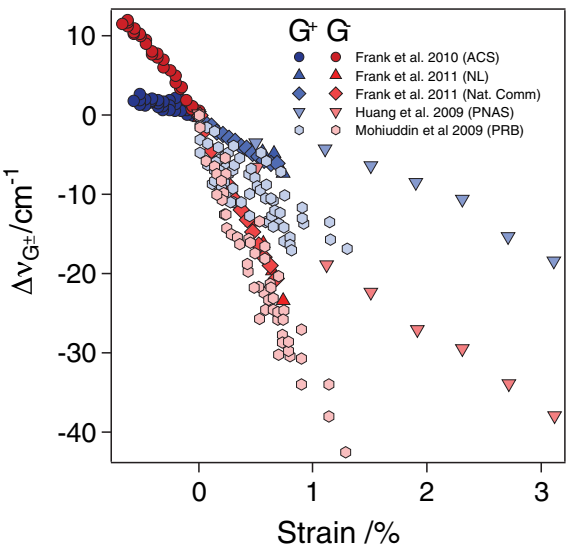

Figure 7. Softening and splitting of the G mode in graphene upon uniaxial stress. Data adapted from several works.[24,54,55,59,62]

longitudinal strain below <0.1%.[54,55,59] Because the G mode is a doubly degenerate phonon mode [TO and longitudinal optical (LO)] with E_{2g} symmetry, for longitudinal strain > 0.1%, this symmetry is broken and the two phonons (TO and LO) coexist and follow their own linear strain dependency.[54,55,62,63] Regarding the 2D mode, the situation is more complex because this mode comes from a second-order double-resonance process and involves two zone boundary phonons. Because of its origin, the 2D mode is dispersive in nature and presents a strong laser energy dependency of about 100 cm^{-1}/eV. Nevertheless, the first Raman studies on the effect of uniaxial strain on the 2D mode show a linear dependency with a slope varying from −21 to −64 cm^{-1}/% of strain depending on the laser excitation energy (Table 1). The discrepancy between these values is too important to be explained only by the 2D mode dispersion. This discrepancy has been clarified using polarized Raman spectroscopy, which reveals the splitting of the 2D modes under uniaxial strain.[63] This study has been followed by others where the splitting was confirmed and reveals the nature of the Raman process involved on the 2D mode components (Table 2).[61–63] Moreover, the slope of the 2D mode dependency with strain is two to three times more important than that of the G band in graphene. As for the G band, the shift in wavenumber is due to bond deformation. In addition to that, the double-resonance Raman process of the 2D mode is highly sensitive to any slight distortion of the Brillouin zone, which strongly modifies the double-resonance conditions and thus enhances the strain effect on the 2D mode. More precisely, under uniaxial stress, the Brillouin zone is distorted and the distance between K and K′ changes.[64–66] Because the 2D Raman process is an inter-valley process, this distance modification induces a higher sensitivity of this mode to uniaxial strain than in the case of the G mode.[54] The same effect should be observed for all defect-assisted modes.

However, the adhesion of graphene on its substrate is indeed known to vary depending on the substrate, and possibly as well depending on how intimate is the contact between the two materials, which may vary depending on the details of the preparation. For instance, adhesion energies on the order of a few 100 mJ/m^2 have been reported on copper[67,68] and SiO_2,[69] of a few 10 mJ/m^2 on cobalt[70] and polydimethylsiloxane[71] and as low as a few 0.01 mJ/m^2 on polyethylene terephthalate.[72] In the latter case, graphene being a deformable membrane, it actually was argued to buckle under stress, as can be expected.[73] From this, we conclude that the experimental reports of values of Raman shift variations with respect to unit strain are possibly in some cases underestimated, owing to slippage or buckling of graphene under interfacial stress, hence effectively more limited stretching/compression of the carbon bonds than intended was applied.[74]

The consequences of uniaxial stress on the Raman spectra of graphene are important and can be listed as follows:

- The presence of uniaxial stress in graphene breaks the symmetry and lifts the degeneracy of the G band (cf. Fig. 7), resulting in two modes G^+ and G^-. The wavenumber difference between these two modes depends on the strain value.
- The displacements associated to G^- and G^+ modes are orthogonal: u_{G+} is perpendicular to the direction of the applied stress, while u_{G-} is parallel to the stress axis. This property is responsible for a faster decrease of the G^- mode wavenumber compared to the G^+ mode under strain. The extreme case is that of the carbon nanotube where the curvature lifts the degeneracy of the two modes LO and TO (usually named G^+ and G^-).[75]
- A direct consequence of the orthogonality of the two G modes is that they are sensitive to the polarization of light in an opposite manner, as shown in particular in the work of Huang *et al.*[59] or Mohiuddin *et al.*[54] Thus, a polarized Raman measurement will select separately the contribution of these two modes and can allow to determine the crystalline orientation of graphene by tuning the in-plane polarization of the incident light.
- The compression and the tensile strain do not have a symmetrical effect on the mode wavenumbers. The wavenumbers of the G^+ and G^- bands decrease when graphene is elongated and increase in compression.
- The 2D mode dependency with strain is two to three times more important than for the G band in graphene because of its high sensitivity to any slight variation of its double-resonance conditions.

Moreover, from the elasticity tensor relating the strain tensor to the stress tensor (Hooke's law), the in-plane Young modulus can be derived. For example, in the case of uniaxial strain on graphene, the diagonal elements of the elasticity tensor correspond to the Young modulus of graphene, and it was then estimated to be $E_{\text{graphene}} \in [1.0; 2.4\ \text{TPa}]$,[76,77] which is of the same order of magnitude as other graphitic systems like carbon nanotubes $E_{\text{nanotube}} \sim 1.25$ TPa[78] or graphite $E_{\text{HOPG}} \sim 1.02$ TPa (in plane).[79] It is also possible to extract the Grüneisen parameter.[54,55,62,63,80] Such a high value is reminiscent of the high in-plane strength of the sigma bonds. However, it is also extracted from a bulk model in which the exact thickness of a monolayer graphene membrane is approximated to the graphite interlayer. Moreover, built-in strain is usually very high in fabricated membranes and drives the system out of the linear stress–strain response giving access to the elastic modulus. Furthermore, graphene naturally exhibits ripples.[81] Upon external stress, two mechanical processes are hence expected. The first one corresponds to the flattening of the graphene ripples; the second one corresponds to the

Table 2. Shift rates of $2D^+$ and $2D^-$ components of the 2D band with uniaxial stress

Graphene orientation/ strain direction	Substrate	$\partial\omega_{2D+}/\partial\epsilon$ (cm^{-1}/%)	$\partial\omega_{2D-}/\partial\epsilon$ (cm^{-1}/%)	Strain interval	Light polarization (P)	λ (nm)	References
Zigzag	PDMS	−16.3	−29.7	Uniaxial $\in [0, 3.2\%]$	P// ϵ	532	Huang *et al.*[63]
Armchair	PDMS	−21.7	−30.5	Uniaxial $\in [0, 3.8\%]$	P// ϵ	532	Huang *et al.*[63]
Zigzag	PMMA	−23.6± 3.6	−46.8 ± 2.1	Uniaxial $\in [0.2\%, 0.6\%]$	P// ϵ	785	Frank *et al.*[62]
Armchair	Acrylic	−44.1	−63.1	Uniaxial $\in [0, 4\%]$	N/A	514.5	Yoon *et al.*[61]
Zigzag	Acrylic	−26	−67.8	Uniaxial $\in [0, 4\%]$	N/A	514.5	Yoon *et al.*[61]

N/A, not applicable; PDMS, polydimethylsiloxane; PMMA, poly(methyl methacrylate).

Table 3. Shift rates of G and 2D modes and their Grüneisen parameters with biaxial strain

Graphene @	$\partial\omega_G/\partial\epsilon_{//}$ (cm^{-1}/%)	$\partial\omega_{2D}/\partial\epsilon_{//}$ (cm^{-1}/%)	Strain	λ (nm)	γ_G	γ_{2D}	References
Shallow depressions	-77 ± 7	-203 ± 20	$\epsilon_{//} = \epsilon_{\perp} = 0.07\%$	632.8	2.4±0.2	3.8±0.3	Metzger *et al.*[83]
PMN_PT piezoelectric	−57	−160.3	$\epsilon_{//} \in [-0.15, 0.10\%]$	532	N/A	N/A	Ding *et al.*[84]
Bubbles	−57	−140	$\epsilon_{//} \in [0, 2\ bar]$	488	1.8±10%	2.6±5%	Zabel *et al.*[85]
Bubbles	−70	N/A	$\epsilon_{//} \in [0.07, 0.19\%]$	514.5	2.2	N/A	Lee *et al.*[86]
Cruciform polymer substrates	-62 ± 5	-148 ± 6	$\epsilon_{//} \in [0, 0.3\%]$	514.5	1.97 ± 0.15	2.86 ± 0.12	Androulidakis *et al.*[80]
Anvil diamond cell	-57.3 ± 0.2	N/A	$\epsilon_{//} \in [-1.5, 0\%]$	532	N/A	N/A	Bousige *et al.*[87]

N/A, not applicable.

extension of the carbon–carbon bonds, which is detected in Raman spectroscopy and related to the position of the G and 2D modes. Nicholl *et al*. showed that, indeed, the former process contributes significantly to the apparent stiffness of the material and should be carefully considered to reliably assess actual stiffness and hence Young's modulus.[82]

The case of biaxial stress

Because graphene prepared by chemical vapor deposition (CVD) on large surfaces is considered to be used as screens, coatings or filters, understanding biaxial deformation is particularly relevant for graphene membranes at all scales. Actually, for these applications, understanding graphene mechanical behavior under a biaxial deformation is mandatory. Moreover, from a fundamental point of view, uniaxial strain modifies the electronic structure of graphene. Because biaxial strain is often relevant to describe the substrate–graphene interaction, the study of biaxial strain effects on the graphene optical phonons is important. In Table 3, a summary of studies on biaxial stress shows that the G mode and 2D mode wavenumbers vary linearly with the strain up to 1.5%, which indicates that slippage and corrugation of the graphene are not involved during these experiments. Moreover, no peak splitting is observed because the applied stress is biaxial. However, the attained strain values in these different experimental works are still low to completely avoid a possible 2D mode splitting, whereas for the G mode, no splitting is theoretically expected in an applied biaxial stress.

The effect of interaction with the substrate: strain or doping effect

On a substrate, not only interfacial stress effects are experienced by graphene, but also charge transfers. Figure 8 shows the dependency of the G mode and its width on the substrate nature. The wavenumber, the width and the intensities of the G mode are strongly different from one substrate to another.

Indeed, strain in CVD or epitaxial graphene is a natural consequence of the growth conditions, thermal expansion differences and interaction between the graphene and the substrate. Moreover, this strain is not automatically released upon transferring graphene to a new substrate as shown in Fig. 8. In the case of CVD graphene grown on copper, the graphene generally exhibits compressive strain owing to the mismatch of thermal expansion

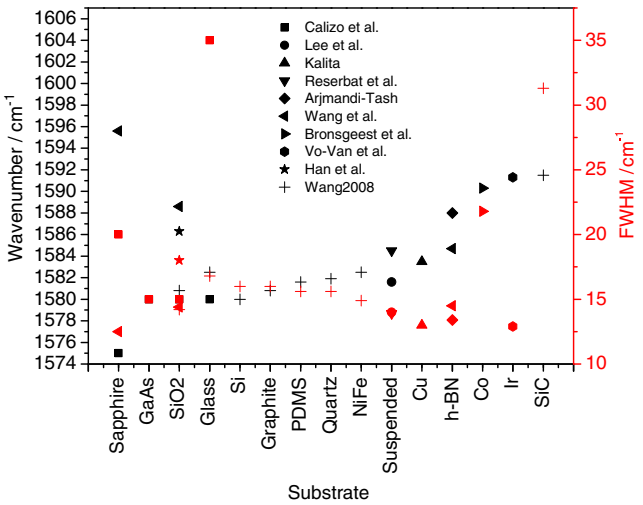

Figure 8. Wavenumber and full width at half maximum of the G mode of graphene deposited on different substrates obtained either by direct growth (Kalita *et al.*,[108] Bronsgeest *et al.*,[70] Vo-Van *et al.*[147] and Wang *et al.* for SiC[148]) or after transfer.[77,103,148–152]

coefficients of copper and graphene. This thermally induced compressive strain was determined to take values of a few percents[68,88] and can be partially relaxed by wrinkle formation. On the other hand, the transferred graphene (because of the very low bending rigidity of graphene) conforms to surface corrugations of the receiving substrate, which can lead to high local strain values on lateral length scales down to a few nanometers.[89,90] The case of metal surfaces is of particular interest because their crystallinity tends to favor well-defined graphene support contacts, which are sources of interfacial stress. Such stress is in particular expected when the metal is used as a catalyst and substrate for graphene growth, for instance, by CVD.

Nevertheless, the electronic interaction between graphene and the metal, even when it is limited, may completely prevent the observation of the Raman modes. A suppression of the Kohn anomaly, in the case of metal surfaces having a similar symmetry to that of graphene, has for instance been invoked to explain the absence of an observable Raman signature for Ni(111), Ru(0001) and Ir(111) substrates.[91–94] The characteristic G and 2D modes are restored in case of an oxygen layer intercalated between graphene and the metal substrate.[95–97]

Graphene prepared on a metal usually exhibits signatures of compressive strain, in the form of a stiffening of the G and 2D modes compared to graphene prepared by mechanical

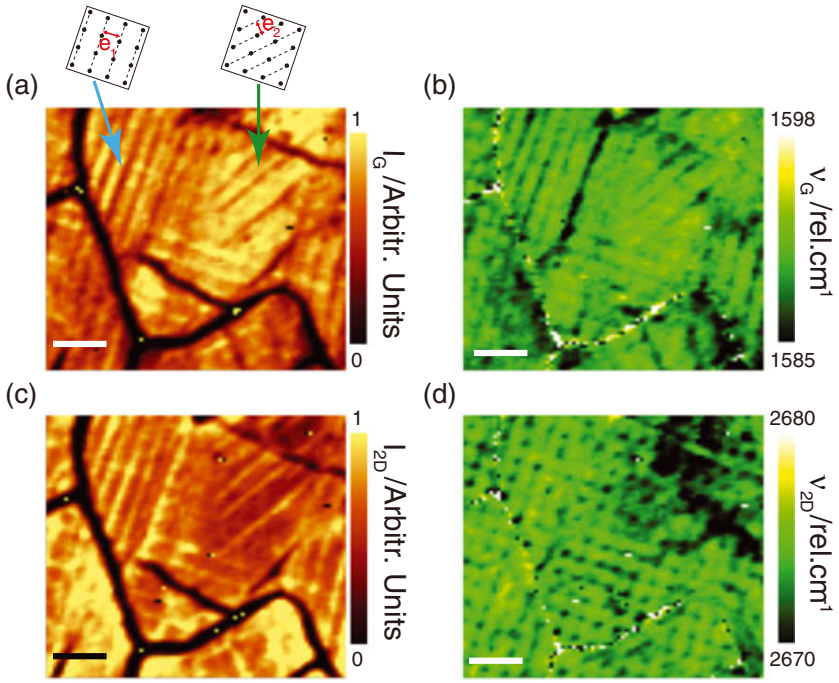

Figure 9. G and 2D wavenumber maps resulting from spatially resolved Raman measured with a 532 nm wavelength laser of graphene deposited on a corrugated substrate. From a ripple region to a flat one in the graphene membrane, the strain difference is about 0.1% and corresponds to a stretching of the graphene locally. Reprinted with permission from Reserbat-Plantey *et al.*[103] Copyright 2010 American Chemical Society.

exfoliation.[98] This stiffening was found to be stronger when the temperature used to grow graphene is higher, which points to the mismatch of the thermal expansion coefficient of graphene and the metal, yielding a thermal stress building up between the growth temperature and room temperature. Metal surfaces with symmetry different from that of graphene, for example, a (100) surface of a face-centered cubic metal like copper, were reported to induce an anisotropic strain in graphene, visible as larger 2D Raman features.[99]

The thermal stress on metal surfaces yields nonuniform strain fields in graphene on metals, owing to the presence of surface features that break the symmetry of graphene. Such features are for instance graphene edges or the natural delimitation of graphene, in the form of wrinkles, which release part of the thermal stress. Bronsgeest *et al.* found that wrinkles and graphene edges impose distinct boundary conditions for graphene, a free-to-slide and a pinned configuration, respectively.[100] A uniaxial strain field results in typically 10% strain variations across microns, which is detected by spatially resolving the position of the G and 2D modes (and discriminating electron doping effects).

We can also monitor the strain by controlling the substrate geometry and thus the graphene properties, which is crucial for applications. For this purpose, some groups try to suspend graphene over a large area of nano-pillars and to accordingly control ripple formation by changing the periodicity of the pillar array. Devices with novel functionalities emerging from the spatial periodicity of the stress have been conceived.[101–103] More specifically, Reserbat-Plantey *et al.*[103] have shown that Raman spectroscopy is an ideal tool to characterize stress-engineered graphene: One can describe the wrinkle induced by the pillars and their symmetry but also the stress domains that correspond to regions of parallel ripples. Because the observed strain is uniaxial, by measuring the G mode and 2D mode wavenumbers, one can access the magnitude of stress at a ripple that is about 1 GPa ($\epsilon \sim 0.1\%$) (Fig. 9).

Finally, if the lattice parameter of the pillar array is reduced, graphene may be fully suspended. This argument also applies to a random network of pillars, suggesting a possible suspension of graphene for a less dense network. Using a corrugated substrate, we can engineer the strain in graphene, which is a key to modulate its electronic and magnetic properties.[104,105] Nevertheless, the question of the strain amplitude and field on a freely suspended graphene also has to be discussed.

However, strain is not the only parameter that can explain the variability of the Raman spectra of graphene with substrate nature. In fact, as described in early works on graphene on SiO_2, the substrate can transfer charges to graphene. As we have seen in the previous section, because of a strong electron–phonon coupling in graphene, charge transfer (or doping) can also significantly influence the optical phonons that are probed by Raman spectroscopy. Moreover, Tiberj *et al.*[106] show that the charge carrier density in graphene on SiO_2 can be tuned from hole to electron doping just by tuning the laser excitation power and consequently modifying the wavenumbers and the width of the G band. Thus, in order to fully describe the influence of the substrate on the Raman spectrum of graphene, we need to disentangle strain and doping effect in the Raman response of graphene, whatever the substrate nature.

Deconvolution of mechanical strain and charge doping by Raman spectroscopy

The deconvolution of strain and doping has been pointed out by the work of Lee *et al.*[77] They show a correlation between the Raman shifts of the G and 2D modes that allows us to disentangle strain and doping. The behavior of the G and 2D Raman

Journal of RAMAN SPECTROSCOPY

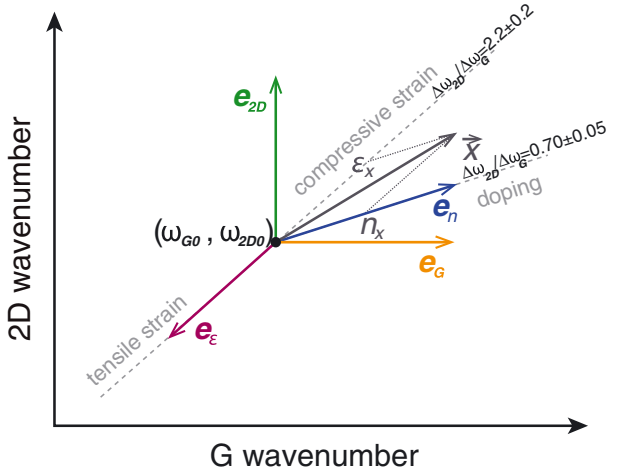

Figure 10. Deconvolution of doping and strain by correlation analysis of the Raman G and 2D mode wavenumbers. Measuring the G and 2D modes at one point of the graphene sample allows to trace a vector $\vec{\mathbf{x}}$ in the (G, 2D) wavenumber plane. Its coordinates, which are known in the orthogonal base given by the vectors $\vec{\mathbf{e}}_\mathbf{G}$ and $\vec{\mathbf{e}}_\mathbf{2D}$, can be projected onto the nonorthogonal vectors $\vec{\mathbf{e}}_\epsilon$ and $\vec{\mathbf{e}}_\mathbf{n}$, which define the components ϵ_x and n_x of vector $\mathbf{x}$ in terms of strain and doping, respectively. The origin of the coordinate system, denoted $(\omega_{G0}, \omega_{2D0})$, is defined by the G and 2D mode wavenumbers for unstrained and undoped graphene. When moving along the strain line towards higher (lower) G and 2D wavenumbers, the compressive (tensile) strain increases.

modes under charge doping has been extensively studied.[7,9–19] The work of Das *et al.* indicates an average ratio of 2D to G mode shifts of $(\Delta\omega_{2D}/\Delta\omega_G)_{\text{hole}} = 0.7$ for hole doping up to a charge density of $2 \cdot 10^{13}$ cm^{-2}. In case of electron doping, the ratio shows slightly lower values in the literature. In contrast, under biaxial mechanical strain, Ding *et al.* measure a G-to-2D shift ratio at about $(\Delta\omega_{2D}/\Delta\omega_G)_{\text{biaxial}} = 2.8$ for both tensile and compressive strains. From one set of G and 2D mode positions (ω_G, ω_{2D}), one can define a vector $\mathbf{x}$ with the origin $(\omega_{G0}, \omega_{2D0})$ as sketched in Fig. 10. This origin is chosen as the undoped and unstrained graphene point.

In order to extract the strain and doping, the vector $\mathbf{x}$ is projected onto the nonorthogonal basis $(\mathbf{e}_\epsilon, \mathbf{e}_n)$ defining the lines along which pure strain and pure doping occur respectively. This can be achieved by a simple coordinate transformation as follows. The strain and doping vectors are known in terms of their components in the space spanned by the orthogonal vectors $\mathbf{e}_G$ and $\mathbf{e}_{2D}$ as depicted in Fig. 10:

$$\begin{pmatrix} \vec{\mathbf{e}}_\epsilon \\ \vec{\mathbf{e}}_\mathbf{n} \end{pmatrix} = \begin{pmatrix} s_G & s_{2D} \\ p_G & p_{2D} \end{pmatrix} \cdot \begin{pmatrix} \vec{\mathbf{e}}_\mathbf{G} \\ \vec{\mathbf{e}}_\mathbf{2D} \end{pmatrix} \tag{5}$$

where the matrix elements denote the shifts of the G and 2D mode positions as a function of biaxial strain and hole doping[77,84]:

$$\begin{aligned} s_G &= \frac{\Delta\omega_G}{\Delta\epsilon} = -57.3 \text{ cm}^{-1}/\% \\ s_{2D} &= \frac{\Delta\omega_{2D}}{\Delta\epsilon} = -160.3 \text{ cm}^{-1}/\% \end{aligned} \tag{6}$$

$$\begin{aligned} p_G &= \frac{\Delta\omega_G}{\Delta n} = 1.0 \cdot 10^{-12} \frac{\text{cm}^{-1}}{\text{cm}^{-2}} \\ p_{2D} &= \frac{\Delta\omega_{2D}}{\Delta n} = 0.7 \cdot 10^{-12} \frac{\text{cm}^{-1}}{\text{cm}^{-2}} \end{aligned} \tag{7}$$

By inverting Eqn (5), one can express the vectors along the measured G and 2D axes as a function of $\vec{\mathbf{e}}_\epsilon$ and $\vec{\mathbf{e}}_\mathbf{n}$:

$$\begin{pmatrix} \vec{\mathbf{e}}_\mathbf{G} \\ \vec{\mathbf{e}}_\mathbf{2D} \end{pmatrix} = \frac{1}{s_G p_{2D} - s_{2D} p_G} \begin{pmatrix} p_{2D} & -s_{2D} \\ -p_G & s_G \end{pmatrix} \cdot \begin{pmatrix} \vec{\mathbf{e}}_\epsilon \\ \vec{\mathbf{e}}_\mathbf{n} \end{pmatrix} \tag{8}$$

With this information, we can express an arbitrary measured vector $\vec{\mathbf{x}} = \mathbf{x_G}\vec{\mathbf{e}}_\mathbf{G} + \mathbf{x_{2D}}\vec{\mathbf{e}}_\mathbf{2D}$ in terms of its strain and doping components:

$$\vec{\mathbf{x}} = \frac{x_G p_{2D} - x_{2D} p_G}{s_G p_{2D} - s_{2D} p_G} \vec{\mathbf{e}}_\epsilon + \frac{x_{2D} s_G - x_G s_{2D}}{s_G p_{2D} - s_{2D} p_G} \vec{\mathbf{e}}_\mathbf{n} \tag{9}$$

Using this approach allows us to extract strain and doping level.[77,100,103,107] This method shows its universal character for a low strain value ($\epsilon < 1.1\%$). However, in the case of metal substrate, the strain field can reach higher strain than in the Lee diagram hypothesis. Thus, for an applied stress that induces the splitting of the G and/or 2D modes, a better model is needed to be able to extract quantitatively the strain and the doping on the studied sample. Recently, Mueller *et al.* propose an experimental methodology to extract the hydrostatic strain and the shear strain by using the average positions of the G and 2D modes together with the splitting value of the two modes.[109] However, in both methodologies (the Lee diagram and the Lee–Mueller diagram), we only have access to global strain and doping values within the sample. In the following section, a methodology is proposed to extract strain and doping maps in order to obtain insights on the spatial distribution on a given sample.

Since the first works on suspended graphene, experimental and theoretical studies have shown that suspended graphene membranes present a low amount of doping in comparison with the supported one, making them suitable to investigate the unique electronic properties of graphene close to electronic neutrality.[85,110] However, these studies also show that suspended graphene exhibits certain corrugations such as ripples, wrinkles, folds or grain boundaries, which can extend over several microns and alter these properties.[81,111]

To suspend graphene, several methods can be employed, for example, mechanical exfoliation on preformed trenches[85,110,112,113] or transfer of large-area graphene obtained by CVD on microstructured substrates.[83,103,114,115] In general, any preparation step altering the surface of graphene can be expected to modify the charge carrier density of graphene, in average or locally. Such effects are hence expected with resist-based wet transfer of CVD-produced graphene or when post-processing steps are needed, for instance, to design electrodes. It is noteworthy that the close-to-charge-neutrality state of graphene may be recovered by annealing graphene, for example, using the Joule effect.[112] We also note that graphene prepared by CVD is expected to exhibit strain inhomogeneities, as we have already discussed, that are at least partly conserved during the transfer process. However, as mentioned previously, Raman spectroscopy allows us to access the amount of strain by using diagram proposed by Lee et al.[77]

As an illustration, Fig. 11a shows such a diagram obtained for a given graphene membrane. More conventionally, regarding the

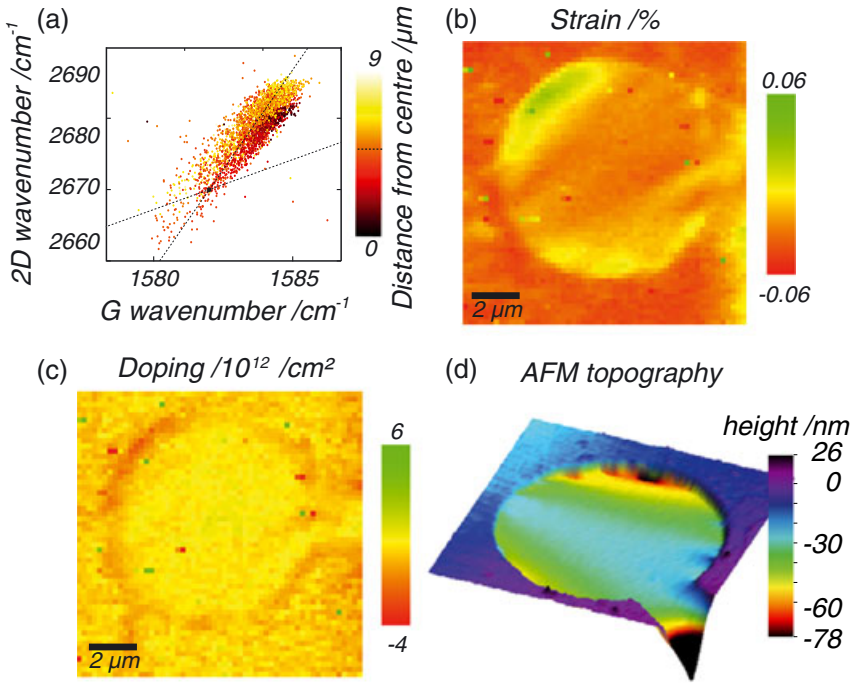

Figure 11. Strain and charge doping analysis with complementary atomic force microscopy (AFM) and Raman measurements. (a) Analysis of Raman G and 2D mode wavenumber correlation as a function of distance from the center of the membrane. The color of each dot indicates the distance of the probed spot from the center of the membrane. The color distribution gives a first hint about the spatial strain distribution in the membrane: The area close to the center (dark spots) nearly superimposes with the area far from the center (bright spots) where the graphene is supported by the substrate. (b, c) Strain and doping maps extracted from panel a. While the doping level is rather homogeneous over the whole measured region, the strain distribution displays local variations that can be understood in terms of the topography of the membrane. (d) AFM height images. Data extracted from Schwarz *et al.*[107]

G and 2D mode wavenumbers, we can observe an overall mode stiffening in the supported regions. However, the effect is more pronounced for the 2D mode, with shifts in the order of 3 to 7 cm^{-1} reflecting its higher sensitivity to strain compared to the G mode (Tables 1 and 2).[11,84,86,116] This result, in addition to the fact that data points in the diagram are aligned (Fig.11a), showing a pure strain line, confirms the existence of strain distribution even on the suspended graphene. Moreover, this observation implies a strain dispersion within the membrane but a constant low doping level, in agreement with previous studies.[85,110]

Moreover, by computing the G mode position vs 2D mode position diagram, we can generate spatial maps for the strain and for the doping distribution as shown Fig.11b,c. In order to extract the exact values of strain and doping, the origin for undoped and unstrained graphene in the diagram needs to be known. Most of the experimental studies in the literature use the origin provided by Lee, which is an extrapolation value.[77] For the work presented here, we define an origin experimentally thanks to a standard CVD graphene suspended over macroscopic length scales (some tens of microns) and supported by a regular array of SiO_2 nano-pillars as detailed in a previous work.[103] This defined origin is reasonable in this case for two reasons: (1) the suspended membrane shown here comes from the same source (same CVD process), and (2) in the macroscopically suspended graphene, only about 10% of the graphene is in direct contact with the substrate.[103] Thus, the origin coordinates (found by averaging over several spectra taken in different regions of a macroscopically suspended monolayer graphene sheet) are given by $(\omega_{G_0}, \omega_{2D_0})$ = (1582 cm^{-1}, 2670 cm^{-1}) (intersection of dashed lines in Fig. 12b). Thus, the extracted strain map shows a low compressive strain in the center region of about 0.04% to 0.03%, which is close to the slightly higher compressive strain in the supported region of about 0.05% to 0.06%. Interestingly, the strain becomes less compressive in general when approaching the membrane edge and even turns to tensile in the regions where the graphene deeply sinks into the hole (as visible in the atomic force microscopy topography, Fig. 11d). These results imply that stress up to about 600 MPa is exerted on the graphene membrane at its circumference where it is attached to the substrate. This tensile stress at the edge counteracts the intrinsic compressive strain that remains after the CVD growth. A similar spatial strain distribution was observed by Reserbat-Plantey *et al.*,[117] who found maximum strain at the clamping point of a multilayer graphene cantilever resonator. Regarding the doping map in Fig. 11c, the doping level is very low (about a few 10^{12} cm^{-2}) throughout the whole graphene membrane and slightly lower in the suspended region as previously described by Berciaud *et al.*[110] However, a quantitative determination of the doping is difficult at such low doping levels, as the anomalous G mode softening occurring at $q = 0$ (as explained in the electron–phonon section) leads to a nonlinear relation between the G mode wavenumber and doping level.[86]

Finally, we want to discuss statistically the differences between suspended and supported graphene in order to test the validity of the fact that suspended graphene is less doped and strained compared to the supported one. As an illustration, Fig. 12a presents typical Raman spectra of a CVD graphene sample transferred onto a 500-nm-thick silica with pre-patterned holes taken in the suspended and supported regions. We notice that the G and 2D mode intensities differ for both cases owing to the optical cavity formed by graphene and the silicon substrate.[118] The absence

Journal of RAMAN SPECTROSCOPY

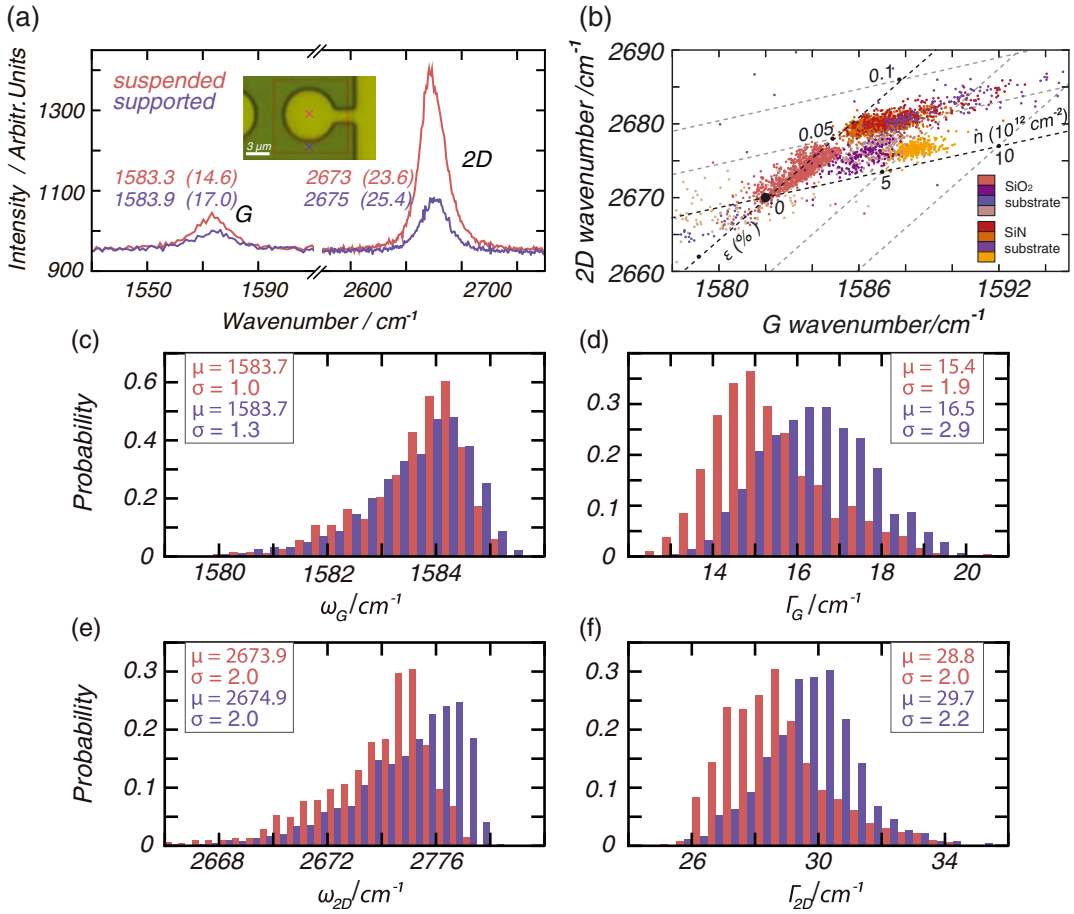

Figure 12. Relative effect of doping and strain on optical phonons of suspended and supported graphene. (a) Comparison of Raman spectra on the supported and suspended graphene. Inset: Optical image of the graphene membrane; the red and blue crosses indicate the positions where the Raman spectra were taken. (b) 2D mode position vs G mode position diagram for several suspended graphene membranes. (c, d) Histogram of G mode wavenumber and width over the graphene membrane presented in the inset of panel a. (e, f) Histogram of 2D mode wavenumber and width of the graphene membrane presented in the inset of panel a. The mean values μ and standard deviations σ of the histograms are reported in units of per inverse centimeters in the legends. While the Raman shift of the G mode hardly changes, the 2D mode wavenumber is on average up-shifted by about 1 cm^{-1} in the supported region. The full width at half maximum decreases for both modes in the suspended region by about 1 cm^{-1}. Data extracted from Schwarz *et al.*[107]

of a significant D peak demonstrates the high structural quality of the transferred CVD graphene (not shown). From the statistics obtained on the shown membrane (Fig. 12c–f), we find that the wavenumber of the G mode does not change noticeably when decoupled from the substrate. It takes an average value of 1583.7 $cm^{-1}\pm1.3$ cm^{-1} in both cases. On the contrary, the 2D mode down-shifts on average by 1 cm^{-1} from supported to suspended graphene. Moreover, the G (2D) mode width ranges from 16.5 cm^{-1} (29.7 cm^{-1}) in the supported region to 15.4 cm^{-1} (28.8 cm^{-1}) in suspended graphene. This implies a longer phonon lifetime in graphene decoupled from the substrate. Moreover, the larger 2D mode width observed in our samples is due to the variation of strain within the sub-micron, which influences the width of the Raman modes as described by Neumann *et al.*[119] At least these statistics indicate that it is very difficult to generalize suspended graphene properties without knowing the residual doping and strain in each specific sample. In fact, obtaining suspended graphene samples with a high success rate is not an easy task; thus, most of the studies on suspended graphene present result on a single graphene sample. To our knowledge, even if most of the studies try to give an overview of the sample (as illustrated earlier), there is only few cases that compare a batch of several samples, allowing to reach statistically relevant conclusions regarding the doped and/ir strained character of suspended graphene.

Figure 12b shows a statistical 2D mode position vs G mode position diagram collecting the data taken with eight different samples of CVD graphene (four suspended membrane over SiO_2 and four others over a SiN substrate). This diagram shows that from sample to sample the strain and the doping levels change strongly. The membranes on SiO_2 show only a strain effect with a very low amount of doping, whereas the membranes on SiN show a lower strain value but a higher doping effect. We also notice, in this diagram, that the Raman peak positions acquired on a given membrane are grouped in elongated clusters that are parallel to the vectors defining either pure doping or pure strain. The Raman results presented here hint to the fact that compressive strain is maintained at lower values up to 0.07% in the graphene membrane even after transfer onto another substrate. Although the difference between the suspended and supported regions is small in general, slightly higher mean values for both strain (−0.029 as compared to −0.023%) and doping (1.0 as compared to 0.7 10^{-12}

cm^{-1}) are found for the graphene in direct contact with the SiO_2 substrate (not shown). The fact that the suspended graphene is also doped can be explained by resist residues that remain on the surface from the transfer process, by doping from air exposure, by charge transfer from the substrate to the suspended graphene or because of the way graphene adheres on the substrate on the sides of the hole. However, this diagram shows that, by using the same CVD graphene and the same transfer conditions, the properties of the suspended graphene depend on the substrate on which it is deposited. This methodology can be applied to graphene whether it is on a substrate or not. However, at larger amounts of strain as briefly discussed in the case of graphene on cobalt, the G mode and/or the 2D mode can split. In this specific case, the recent approach developed by Mueller *et al.*[109] has to be applied. The role of strain can be crucial in modifying the graphene properties on purpose, but its characterization is also required as a starting point in order to use the mechanical properties of graphene in a device. In the next section, we show how to use this optical phonon dependency with strain and/or doping for applications.

Application: optomechanics of graphene and molecular detection

As mentioned earlier, Raman spectroscopy is highly sensitive to strain and a valuable alternative to standard reflectometry characterizations of mechanical oscillators based on sp^2 carbon allotropes or other low-dimensional systems such as SiC nanowires, providing fine insights into local strains and the effect of mechanical resonances.[117] At the nanometer scale, mechanical resonators offer new possibilities to study mechanics and develop new probes for condensed matter. Their resonance frequency is in the range of megahertz to gigahertz, and detecting motion of the resonator requires a strong and fast coupling between the mechanical movement and another object or particle including (1) electrons (capacitive coupling,[120–122] magnetism,[123–125] tunneling,[126] and piezoelectricity[127]), (2) atomic force microscopy cantilever[128,129] and (3) photons[130–134] or optical phonons as will be discussed in the following.

Moreover, because of their low dimension, an inhomogeneous distribution of stress in these systems induces a deeper modification of their mechanical properties and thus a modification of their operation.[135] It is therefore necessary to measure the strain distribution in both static and dynamic regimes in order to understand the dissipation processes, which limits the quality factor of these resonators.

A major issue in this field is still the difficulty to detect and map the mechanical properties of a nanoelectromechanical system (deformation and stress). This difficulty is mainly due to the fact that the transduction of these into a measurable signal requires a strong coupling between the probe (photons, electrons, etc.) and displacement or mechanical stress. The coupling between a mechanical resonator and a cavity amplifies this signal and thereby allows the detection of the movement or the manipulation of the resonator state.[136] The early work of Bunch *et al.* in 2007 shows the coupling between photons and a graphene resonator doubly clamped for movement detection.[134] This detection is possible thanks to an optical cavity formed by the graphene membrane and the silicon surface underneath which thus forms a Fabry–Pérot interferometer. With this interferometric detection, Bunch *et al.*[134] reached a strength sensitivity of about 1 fN $Hz^{-1/2}$. Because graphene combines low mass (fg), high resonance frequency (MHz), and high quality factor ($>10^4$), it is an excellent candidate to achieve advances in the sensitivity of mass sensors, force, position or electric charge sensors. Nevertheless, as previously described, its properties are strongly affected by strain. In the following example,[117] by combining the optical interference with Raman scattering, we provide a local and nonperturbative measurement of motion and mechanical strain by interferometric detection and Raman spectroscopy. These systems are simply clamped and perfectly compatible with optical detection.

As can be seen in Fig. 13, the mechanical resonance can be detected using the G mode wavenumber dependency with the applied frequency. We can also convert this wavenumber shift into a strain value and thus extract the value of strain at a resonance that is about 1.6 GPa. This detection probe allows us to consider a new type of optomechanical coupling between acoustic and optical phonons. Actually, at resonance, the deformation amplitude is maximum, and from Hookes law, this corresponds also to maximum strain in the membrane. Again, as for the determination of strain in suspended graphene, different contributions can arise from the bond length and from ripples. However, their combined effects result in a maximum at resonance, which allows for mechanical mode detection, which is applicable to various kinds of membranes.

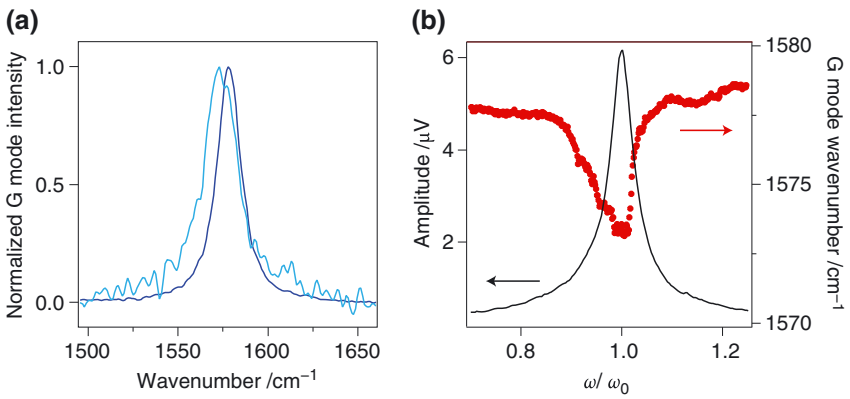

Figure 13. Probing mechanical resonance and stress by Raman spectroscopy. (a) Raman spectra of the G peak of an electrostatically actuated multilayer graphene cantilever at the mechanical resonance frequency (red) and at a frequency 360 kHz lower than the resonance frequency (blue). (b) Amplitude of cantilever oscillations at 2ν (black line, left axis) and Raman shift (green symbols, right axis) *versus* drive frequency in vacuum.

We also demonstrate that this Raman probe of mechanical resonance can be generalized as far as the probed material has an optical phonon sensitive to strain variations. Thus, we can locally probe the motion and the strain on the probed material just by Raman spectroscopy. Recently, the same Raman detection has been achieved for single-layer graphene (not shown). A recent work of Metten *et al.*[137] uses the same optical interference approach to measure strain and doping induced by electrostatic gating, giving rise to the same conclusion on the possibility to drive electrostatically the graphene deflection and be able to measure the strain and the doping induced within the membrane. Moreover, theoretical works[104,105] predict the possibility to tune the graphene properties by strain engineering as already mentioned, such as opening a band gap, but experimentally it is not realized yet, whereas in the case of MoS_2, the possibility to tune the optical band gap of MoS_2 by as much as 500 meV by applying very high biaxial strains has been recently demonstrated by Lloyd *et al.*[138] This first result is very promising, and suggests to explore the possibilities offered various members in the already vast family of 2D materials.

The use of Raman spectroscopy to reveal graphite, nanotube and graphene properties has been a long-term scientific journey starting in the middle of the sixties[139] and still going on up to now. The stability and availability of monolayer graphene open the way to a large panel of applications for which Raman spectroscopy is crucial to identify the structure, the doping and the strain level of graphene. As described in this review, the effects of perturbations on monolayer graphene are essential to understand and implement its properties; for example, strain engineering is a possible route towards inducing strong pseudo-magnetic fields.[105,140–142] In fact, the same effects appear for different 2D materials. A support is required to handle them, and thus, the substrate interaction will play a major role by inducing either doping and/or strain as shown in this review. Actually, a similar doping effect on the optical phonons and the photoluminescence has been already reported on transition metal dichalcogenides.[50–52] Of course, the Raman spectroscopy of the bulk of these 2D materials has been studied many years ago; however, their monolayer counterparts can present very different properties. For example, the MoS_2 monolayer has a direct band gap, whereas the bulk shows an indirect band gap opening the way to a large panel of applications like photodetectors[143] and optoelectronics.[144] This 2D material is now extensively studied by using Raman spectroscopy: Its structure (number of layers and defects) can be described by its optical phonons but also its mechanical properties because its optical phonons depend on the applied strain. Moreover, the combinations of 2D layers in three-dimensional stacks allows to design in purpose a given functionality.[144,145] One could combine conductive, insulating, superconducting or photoactive layers up to three-dimensional crystals, the chosen functionality being intrinsic and inside such heterostructures. Thus, Raman spectroscopy will be a useful tool for probing the functionality and the properties of these heterostructures because their optical phonons are mostly sensitive to external perturbations. Beyond Raman spectroscopy, obtaining a full picture of 2D material properties will require different approaches: by combining Raman spectroscopy and other probes such as electronic transport or mechanical motion, a comprehensive understanding of the physical properties at this dimension can be reached.

Acknowledgement

The authors wish to thank A. Reserbat-Plantey, D. Kalita, and also V. Reita, D. Jegouso and C. Felix for technical support. This work is supported by TRICO (ANR-11-NANO-0025), Cleangraph (ANR-13-BS09-0019), Diracformag (ANR-14-CE32-0003), NC2 (ANR-15-CE30-0010), Organisio (ANR-15-CE09-0017), 2D transformer (ANR-14-OHRI-0004), the European Union H2020 program under the grant 696656 Graphene Flagship and LANEF framework (ANR-10-LABX-51-01).

References

[1] S. Reich, C. Thomsen, *Philos. Trans. R. Soc. London, A: Math., Phys. Eng. Sci.* **2004**, *362*, 2271.
[2] R. Nemanich, G. Lucovsky, S. Solin, *Solid State Commun.* **1977**, *23*, 117.
[3] J. Maultzsch, S. Reich, C. Thomsen, H. Requardt, P. Ordejón, *Phys. Rev. Lett.* **2004**, *92*, 075501.
[4] F. Tuinstra, J. L. Koenig, *J. Chem. Phys.* **1970**, *53*, 1126.
[5] A. C. Ferrari, J. Robertson, *Phys. Rev. B* **2000**, *61*, 14095.
[6] C. Thomsen, S. Reich, *Phys. Rev. Lett.* **2000**, *85*, 5214.
[7] A. C. Ferrari, A. K. Sood, A. Das, S. Pisana, B. Chakraborty, S. Piscanec, S. K. Saha, U. V. Waghmare, K. S. Novoselov, H. R. Krishnamurthy, A. K. Geim, *Nat. Nanotechnol.* **2008**, *3*, 210.
[8] B. M. Kessler, C. Girit, A. Zettl, V. Bouchiat, *Phys. Rev. Lett.* **2010**, *104*, 047001.
[9] A. Das, A. K. Sood, A. Govindaraj, A. M. Saitta, M. Lazzeri, F. Mauri, C. N. R. Rao, *Phys. Rev. Lett.* **2007**, *99*, 136803.
[10] H. Farhat, H. Son, G. G. Samsonidze, S. Reich, M. S. Dresselhaus, J. Kong, *Phys. Rev. Lett.* **2007**, *99*, 145506.
[11] A. Das, S. Pisana, B. Chakraborty, S. Piscanec, S. K. Saha, U. V. Waghmare, K. S. Novoselov, H. R. Krishnamurthy, A. K. Geim, A. C. Ferrari, A. K. Sood, *Nat. Nanotechnol.* **2008**, *3*, 210.
[12] P. M. Rafailov, J. Maultzsch, C. Thomsen, U. Dettlaff-Weglikowska, S. Roth, *Nano Lett.* **2009**, *9*, 3343.
[13] A. W. Bushmaker, V. V. Deshpande, S. Hsieh, M. W. Bockrath, S. B. Cronin, *Nano Lett.* **2009**, *9*, 607.
[14] N. Bendiab, L. Spina, A. Zahab, P. Poncharal, C. Marliére, J. L. Bantignies, E. Anglaret, J. L. Sauvajol, *Phys. Rev. B* **2001**, *63*, 153407.
[15] J. C. Tsang, M. Freitag, V. Perebeinos, J. Liu, P. h. Avouris, *Nat. Nanotechnol.* **2007**, *2*, 725.
[16] N. Caudal, A. M. Saitta, M. Lazzeri, F. Mauri, *Phys. Rev. B* **2007**, *75*, 115423.
[17] J. Yan, Y. Zhang, P. Kim, A. Pinczuk, *Phys. Rev. Lett.* **2007**, *98*, 166802.
[18] C. Stampfer, F. Molitor, D. Graf, K. Ensslin, A. Jungen, C. Hierold, L. Wirtz, *Appl. Phys. Lett.* **2007**, *91*, 241907.
[19] S. Pisana, M. Lazzeri, C. Casiraghi, K. S. Novoselov, a. K. Geim, A. C. Ferrari, F. Mauri, *Nat. Mater.* **2007**, *6*, 198.
[20] O. Frank, M. S. Dresselhaus, M. Kalbac, *Acc. Chem. Res.* **2015**, *48*, 111.
[21] M. Kalbac, A. Reina-Cecco, H. Farhat, J. Kong, L. Kavan, M. S. Dresselhaus, *ACS Nano* **2010**, *4*, 6055.
[22] W. Kohn, *Rev, Phys. Lett.* **1959**, *2*, 393.
[23] S. Piscanec, M. Lazzeri, F. Mauri, A. C. Ferrari, J. Robertson, *Phys. Rev. Lett.* **2004**, *93*, 1.
[24] O. Frank, M. Bousa, I. Riaz, R. Jalil, K. Novoselov, G. Tsoukleri, J. Parthenios, L. Kavan, K. Papagelis, C. Galiotis, *Nano Lett.* **2012**, *12*, 687.
[25] M. Lazzeri, F. Mauri, *Phys. Rev. Lett.* **2006**, *97*, 266407.
[26] J. Yan, E. A. Henriksen, P. Kim, A. Pinczuk, *Phys. Rev. Lett.* **2008**, *101*, 136804.
[27] D. M. Basko, S. Piscanec, A. C. Ferrari, *Phys. Rev. B* **2009**, *80*, 165413.
[28] C.-F. Chen, C.-H. Park, B. W. Boudouris, J. Horng, B. Geng, C. Girit, A. Zettl, M. F. Crommie, R. A. Segalman, S. G. Louie, F. Wang, *Nature* **2011**, *617*, 471.
[29] E. H. Hasdeo, A. R. T. Nugraha, M. S. Dresselhaus, R. Saito, *Phys. Rev. B* **2016**, *94*, 1.
[30] D. Yoon, D. Jeong, H.-J. Lee, R. Saito, Y.-W. Son, H. C. Lee, H. Cheong, *Carbon* **2013**, *61*, 373.
[31] E. H. Hasdeo, A. R. T. Nugraha, M. S. Dresselhaus, R. Saito, *Phys. Rev. B* **2014**, *90*, 245140.
[32] T. Ando, *J. Phys. Soc. Jpn.* **2006**, *75*, 124701.
[33] G. Froehlicher, S. Berciaud, *Phys. Rev. B* **2015**, *91*, 205413.

[34] D. L. Mafra, J. Kong, K. Sato, R. Saito, M. S. Dresselhaus, P. T. Araujo, *Phys. Rev. B* **2012**, *86*, 195434.
[35] P. T. Araujo, D. L. Mafra, K. Sato, R. Saito, J. Kong, M. S. Dresselhaus, *Phys. Rev. Lett.* **2012**, *109*, 046801.
[36] C. Casiraghi, *Rev, Phys. B* **2009**, *80*, 233407.
[37] S. Reichardt, L. Wirtz, *Phys. Rev. B* **2017**, *95*, 195422.
[38] L. G. Cancado, A. Jorio, E. H. M. Ferreira, F. Stavale, C. A. Achete, R. B. Capaz, M. V. O. Moutinho, A. Lombardo, T. S. Kulmala, A. C. Ferrari, *Nano Lett.* **2011**, *11*, 3190.
[39] A. Eckmann, A. Felten, A. Mishchenko, L. Britnell, R. Krupke, K. S. Novoselov, C. Casiraghi, *Nano Lett.* **2012**, *12*, 3925.
[40] J. Liu, Q. Li, Y. Zou, Q. Qian, Y. Jin, G. Li, K. Jiang, S. Fan, *Nano Lett.* **2013**, *13*, 6170.
[41] M. Bruna, A. K. Ott, M. Ijäs, D. Yoon, U. Sassi, A. C. Ferrari, *ACS Nano* **2014**, *8*, 7432.
[42] D.-H. Chae, T. Utikal, S. Weisenburger, H. Giessen, K. Klitzing, M. Lippitz, J. Smet, *Nano Lett.* **2011**, *11*, 1379.
[43] K. F. Mak, F. H. Da Jornada, K. He, J. Deslippe, N. Petrone, J. Hone, J. Shan, S. G. Louie, T. F. Heinz, *Phys. Rev. Lett.* **2014**, *112*, 207401.
[44] I. Calizo, I. Bejenari, M. Rahman, G. Liu, A. A. Balandin, *J. Appl. Phys.* **2009**, *106*, 043509.
[45] C. Tyborski, F. Herziger, R. Gillen, J. Maultzsch, *Phys. Rev. B* **2015**, *92*, 041401.
[46] R. Saito, A. R. T. Nugraha, E. H. Hasdeo, S. Siregar, H. Guo, T. Yang, *Phys. Status Solidi (b)* **2015**, *252*, 2363.
[47] I. Brihuega, P. Mallet, H. González-Herrero, G. Trambly de Laissardière, M. M. Ugeda, L. Magaud, J. M. Gómez-Rodríguez, F. Ynduráin, J.-Y. Veuillen, *Phys. Rev. Lett.* **2012**, *109*, 196802.
[48] K. Sato, R. Saito, C. Cong, T. Yu, M. S. Dresselhaus, *Phys. Rev. B* **2012**, *86*, 125414.
[49] K. Kim, S. Coh, L. Z. Tan, W. Regan, J. M. Yuk, E. Chatterjee, M. F. Crommie, M. L. Cohen, S. G. Louie, A. Zettl, *Phys. Rev. Lett.* **2012**, *108*, 246103.
[50] M. A. Pimenta, E. del Corro, B. R. Carvalho, C. Fantini, L. M. Malard, *Acc. Chem. Res.* **2015**, *48*, 41.
[51] M. Buscema, G. A. Steele, H. S. J. van der Zant, A. Castellanos-Gomez, *Nano Res.* **2014**, *7*, 561.
[52] S. Mouri, Y. Miyauchi, K. Matsuda, *Nano Lett.* **2013**, *13*, 5944.
[53] B. Chakraborty, A. Bera, D. V. S. Muthu, S. Bhowmick, U. V. Waghmare, A. K. Sood, *Phys. Rev. B* **2012**, *85*, 161403.
[54] T. M. G. Mohiuddin, A. Lombardo, R. R. Nair, A. Bonetti, G. Savini, R. Jalil, N. Bonini, D. M. Basko, C. Galiotis, N. Marzari, K. S. Novoselov, A. K. Geim, A. C. Ferrari, *Phys. Rev. B* **2009**, *79*, 205433.
[55] O. Frank, G. Tsoukleri, I. Riaz, K. Papagelis, J. Parthenios, A. C. Ferrari, A. K. Geim, K. S. Novoselov, C. Galiotis, *Nat. Comm.* **2011**, *2*.
[56] M. Cardona, Resonant Raman scattering in semiconductors, in *Elementary Excitations in Solids, Molecules, and Atom: Part B* (Eds: J. T. Devreese, A. B. Kunz, T. C. Collins), Springer, Boston, MA, **1974**, pp. 269–291.
[57] M. Hanfland, K. Syassen, S. Fahy, S. G. Louie, M. L. Cohen, *Phys. Rev. B,* **1985**, *31*, 6896.
[58] E. Anastassakis, A. Pinczuk, E. Burstein, F. Pollak, M. Cardona, *Solid State Commun.* **1993**, *88*, 1053.
[59] M. Huang, H. Yan, C. Chen, D. Song, T. F. Heinz, J. Hone, *Proc. Nat. Acad. Sci.* **2009**, *106*, 7304.
[60] Z. H. Ni, T. Yu, Y. H. Lu, Y. Y. Wang, Y. P. Feng, Z. X. Shen, *ACS Nano* **2008**, *2*, 2301.
[61] D. Yoon, Y.-W. Son, H. Cheong, *Phys. Rev. Lett.* **2011**, *106*, 155502.
[62] O. Frank, M. Mohr, J. Maultzsch, C. Thomsen, I. Riaz, R. Jalil, K. S. Novoselov, G. Tsoukleri, J. Parthenios, K. Papagelis, L. Kavan, C. Galiotis, *ACS Nano* **2011**, *5*, 2231.
[63] M. Huang, H. Yan, T. F. Heinz, J. Hone, *Nano Lett.* **2010**, *10*, 4074.
[64] L. Yang, J. Han, *Phys. Rev. Lett.* **2000**, *85*, 154.
[65] F. Herziger, M. Calandra, P. Gava, P. May, M. Lazzeri, F. Mauri, J. Maultzsch, *Phys. Rev. Lett.* **2014**, *113*, 187401.
[66] C. Cong, T. Yu, *Phys. Rev. B* **2014**, *89*, 235430.
[67] T. Yoon, W. C. Shin, T. Y. Kim, J. H. Mun, T.-S. Kim, B. J. Cho, *Nano Lett.* **2012**, *12*, 1448.
[68] O. Frank, J. Vejpravova, V. Holy, L. Kavan, M. Kalbac, *Carbon* **2014**, *68*, 440.
[69] S. P. Koenig, N. G. Boddeti, M. L. Dunn, J. S. Bunch, *Nat. Nanotechnol.* **2011**, *6*, 543.
[70] M. S. Bronsgeest, N. Bendiab, S. Mathur, A. Kimouche, H. T. Johnson, J. Coraux, P. Pochet, *Nano Lett.* **2015**, *15*, 5098.
[71] S. Scharfenberg, D. Z. Rocklin, C. Chialvo, R. L. Weaver, P. M. Goldbart, N. Mason, *Appl. Phys. Lett.* **2011**, *98*, 091908.
[72] T. Jiang, R. Huang, Y. Zhu, *Adv. Funct. Mater.* **2014**, *24*, 396.
[73] P. Lambin, *Appl. Sci.* **2014**, *4*, 282.
[74] A. L. Kitt, Z. Qi, S. Rémi, H. S. Park, A. K. Swan, B. B. Goldberg, *Nano Lett.* **2013**, *13*, 2605.
[75] S. Reich, C. Thomsen, *Phys. Rev. B* **2000**, *62*, 4273.
[76] C. Lee, X. Wei, J. W. Kysar, J. Hone, *Science* **2008**, *321*, 385.
[77] J. E. Lee, G. Ahn, J. Shim, Y. S. Lee, S. Ryu, *Nat. Commun.* **2012**, *3*, 1024.
[78] A. Krishnan, E. Dujardin, T. W. Ebbesen, P. N. Yianilos, M. M. J. Treacy, *Phys. Rev. B* **1998**, *58*, 14013.
[79] O. L. Blakslee, D. G. Proctor, E. J. Seldin, G. B. Spence, T. Weng, *J. Appl. Phys.* **1970**, *41*, 3373.
[80] C. Androulidakis, E. N. Koukaras, J. Parthenios, G. Kalosakas, K. Papagelis, C. Galiotis, *Sci. Rep.* **2015**, *5*, 18219.
[81] J. C. Meyer, A. K. Geim, M. I. Katsnelson, K. S. Novoselov, T. J. Booth, S. Roth, *Nature* **2007**, *446*, 60.
[82] R. J. Nicholl, H. J. Conley, N. V. Lavrik, I. Vlassiouk, Y. S. Puzyrev, V. P. Sreenivas, S. T. Pantelides, K. I. Bolotin, *Nat. Commun.* **2015**, *6*, 8789.
[83] C. Metzger, S. Rémi, M. Liu, S. V. Kusminskiy, A. H. Castro Neto, A. K. Swan, B. B. Goldberg, *Nano Lett.* **2010**, *10*, 6.
[84] F. Ding, H. Ji, Y. Chen, A. Herklotz, K. Dörr, Y. Mei, A. Rastelli, O. G. Schmidt, *Nano Lett.* **2010**, *10*, 3453.
[85] J. Zabel, R. R. Nair, A. Ott, T. Georgiou, A. K. Geim, K. S. Novoselov, C. Casiraghi, *Nano Lett.* **2012**, *12*, 617.
[86] J.-U. Lee, D. Yoon, H. Cheong, *Nano Lett.* **2012**, *12*, 4444.
[87] C. Bousige, F. Balima, D. Machon, G. S. Pinheiro, A. Torres-Dias, J. Nicolle, D. Kalita, N. Bendiab, L. Marty, V. Bouchiat, G. Montagnac, A. G. Souza Filho, P. Poncharal, A. San-Miguel, *Nano Lett.* **2017**, *17*, 21, 28073255.
[88] L. Tapasztó, T. Dumitrică, S. J. Kim, P. Nemes-Incze, C. Hwang, L. P. Biró, *Nat. Phys.* **2012**, *8*, 739.
[89] M. Ishigami, J. H. Chen, W. G. Cullen, M. S. Fuhrer, E. D. Williams, *Nano Lett.* **2007**, *7*, 1643.
[90] S. Ryu, L. Liu, S. Berciaud, Y.-J. Yu, H. Liu, P. Kim, G. W. Flynn, L. E. Brus, *Nano Lett.* **2010**, *10*, 4944.
[91] E. Starodub, A. Bostwick, L. Moreschini, S. Nie, F. El Gabaly, K. F. McCarty, E. Rotenberg, *Phys. Rev. B* **2011**, *83*, 125428.
[92] P. W. Sutter, J.-I. Flege, E. A. Sutter, *Nat. Mater.* **2008**, *7*, 406.
[93] A. Allard, L. Wirtz, *Nano Lett.* **2010**, *10*, 4335.
[94] A. Allard, *Etude ab-initio des phonons du graphène sur substrats métalliques*. PhD thesis, Université, de Lille 1, **2011**.
[95] C. Vo-Van, A. Kimouche, A. Reserbat-Plantey, O. Fruchart, P. Bayle-Guillemaud, N. Bendiab, J. Coraux, *Appl. Phys. Lett.* **2011**, *98*, 181903.
[96] A. Kimouche, O. Renault, S. Samaddar, C. Winkelmann, H. Courtois, O. Fruchart, J. Coraux, *Carbon* **2014**, *68*, 73.
[97] S. Martin, S. Samaddar, B. Sacépé, A. Kimouche, J. Coraux, F. Fuchs, B. Grévin, H. Courtois, C. Winkelmann, *Phys. Rev. B* **2015**, *91*, 041406.
[98] V. Yu, E. Whiteway, J. Maassen, M. Hilke, *Phys. Rev. B* **2011**, *84*, 205407.
[99] R. He, L. Zhao, N. Petrone, K. S. Kim, M. Roth, J. Hone, P. Kim, A. Pasupathy, A. Pinczuk, *Nano Lett.* **2012**, *12*, 2408.
[100] M. S. Bronsgeest, N. Bendiab, S. Mathur, A. Kimouche, H. T. Johnson, J. Coraux, P. Pochet, *Nano Lett.* **2015**, *15*, 5098.
[101] H. Tomori, A. Kanda, H. Goto, Y. Ootuka, K. Tsukagoshi, S. Moriyama, E. Watanabe, D. Tsuya, *Appl. Phys. Express* **2011**, *4*, 075102.
[102] M. Neek-Amal, L. Covaci, F. M. Peeters, *Phys. Rev. B* **2012**, *86*, 041405.
[103] A. Reserbat-Plantey, D. Kalita, Z. Han, L. Ferlazzo, S. Autier-Laurent, K. Komatsu, C. Li, R. Weil, A. Ralko, L. Marty, S. Guéron, N. Bendiab, H. Bouchiat, V. Bouchiat, *Nano Lett.* **2014**, *14*, 5044.
[104] V. M. Pereira, A. H. Castro Neto, H. Y. Liang, L. Mahadevan, *Phys. Rev. Lett.* **2010**, *105*, 156603.
[105] F. Guinea, M. I. Katsnelson, a. K. Geim, *Nat. Phys.* **2009**, *6*, 30.
[106] A. Tiberj, M. Rubio-Roy, M. Paillet, J.-R. Huntzinger, P. Landois, M. Mikolasek, S. Contreras, J.-L. Sauvajol, E. Dujardin, A.-A. Zahab **2013**, *1*, 2.
[107] C. Schwarz, *http://www.theses.fr*. Thesis, Université Grenoble Alpes, **2016**.
[108] C. Dipankar, *http://www.theses.fr*. Thesis, Université Grenoble Alpes, **2015**.
[109] N. S. Mueller, coworkers, arXiv:1703.09592v2, **2017**. arXiv:1703.09592v2.
[110] S. Berciaud, S. Ryu, L. E. Brus, T. F. Heinz, *Nano Lett.* **2009**, *9*, 346.
[111] A. Fasolino, J. H. Los, M. I. Katsnelson, *Nat. Mat.* **2007**, *6*, 858.
[112] K. Bolotin, K. Sikes, Z. Jiang, M. Klima, G. Fudenberg, J. Hone, P. Kim, H. Stormer, *Solid State Commun.* **2008**, *146*, 351.

[113] D. Metten, F. m. c. Federspiel, M. Romeo, S. Berciaud, *Phys. Rev. Applied* **2014**, *2*, 054008.
[114] J. W. Suk, A. Kitt, C. W. Magnuson, Y. Hao, S. Ahmed, J. An, A. K. Swan, B. B. Goldberg, R. S. Ruoff, *ACS Nano* **2011**, *5*, 6916.
[115] S. Chen, Q. Li, Q. Zhang, Y. Qu, H. Ji, R. S. Ruoff, W. Cai, *Nanotechnology* **2012**, *23*, 365701.
[116] A. Das, B. Chakraborty, S. Piscanec, S. Pisana, A. K. Sood, A. C. Ferrari, *Phys. Rev. B* **2009**, *79*, 155417.
[117] A. Reserbat-Plantey, L. Marty, O. Arcizet, N. Bendiab, V. Bouchiat, *Nat. Nanotechnol.* **2012**, *7*, 151.
[118] D. Yoon, H. Moon, Y.-W. Son, J. S. Choi, B. H. Park, Y. H. Cha, Y. D. Kim, H. Cheong, *Phys. Rev. B* **2009**, *80*, 125422.
[119] C. Neumann, S. Reichardt, P. Venezuela, M. Drögeler, L. Banszerus, M. Schmitz, K. Watanabe, T. Taniguchi, F. Mauri, B. Beschoten, S. V. Rotkin, C. Stampfer, *Nat. Comm.* **2015**, *6*, 8429.
[120] V. Gouttenoire, T. Barois, S. Perisanu, J.-L. Leclercq, S. T. Purcell, P. Vincent, A. Ayari, *Small* **2010**, *6*, 1060.
[121] V. Sazonova, Y. Yaish, H. Üstünel, D. Roundy, T. A. Arias, P. L. McEuen, *Nature* **2004**, *431*, 284.
[122] A. Naik, O. Buu, M. D. LaHaye, A. D. Armour, A. A. Clerk, M. P. Blencowe, K. C. Schwab, *Nature* **2006**, *443*, 193.
[123] M. Defoort, K. Lulla, J.-S. Heron, O. Bourgeois, E. Collin, F. Pistolesi, *Appl. Phys. Lett.* **2011**, *99*, 233107.
[124] W. J. Venstra, H. J. R. Westra, K. B. Gavan, H. S. J. van der Zant, *Appl. Phys. Lett.* **2009**, *95*, 263103.
[125] P. Rabl, P. Cappellaro, M. V. G. Dutt, L. Jiang, J. R. Maze, M. D. Lukin, *Phys. Rev. B* **2009**, *79*, 041302.
[126] T. W. Kenny, J. K. Reynolds, J. A. Podosek, E. C. Vote, L. M. Miller, H. K. Rockstad, W. J. Kaiser, *Rev. Sci. Instrum.* **1996**, *67*, 112.
[127] R. G. Beck, M. A. Eriksson, M. A. Topinka, R. M. Westervelt, K. D. Maranowski, A. C. Gossard, *Appl. Phys. Lett.* **1998**, *73*, 1149.
[128] D. Garcia-Sanchez, A. M. van der Zande, A. S. Paulo, B. Lassagne, P. L. McEuen, A. Bachtold, *Nano Lett.* **2008**, *8*, 1399.
[129] D. Garcia-Sanchez, A. San Paulo, M. J. Esplandiu, F. Perez-Murano, L. Forró, A. Aguasca, A. Bachtold, *Phys. Rev. Lett.* **2007**, *99*, 085501.
[130] O. Arcizet, V. Jacques, A. Siria, P. Poncharal, P. Vincent, S. Seidelin, *Nat. Phys.* **2011**, *7*, 879.
[131] D. Karabacak, T. Kouh, K. L. Ekinci, *J. Appl. Phys.* **2005**, *98*, 124309.
[132] D. Karabacak, T. Kouh, C. C. Huang, K. L. Ekinci, *Appl. Phys. Lett.* **2006**, *88*, 193122.
[133] T. Kouh, D. Karabacak, D. H. Kim, K. L. Ekinci, *Appl. Phys. Lett.* **2005**, *86*, 013106.
[134] J. S. Bunch, A. M. van der Zande, S. S. Verbridge, I. W. Frank, D. M. Tanenbaum, J. M. Parpia, H. G. Craighead, P. L. McEuen, *Science* **2007**, *315*, 490.
[135] S. S. Verbridge, J. M. Parpia, R. B. Reichenbach, L. M. Bellan, H. G. Craighead, *J. Appl. Phys.* **2006**, *99*, 124304.
[136] R. a. Barton, I. Storch, V. P. Adiga, R. Sakakibara, B. R. Cipriany, R. Ilic, S. P. Wang, P. Ong, P. L. McEuen, J. M. Parpia, H. G. Craighead, *Nano Lett.* **2012**, 10.1021/nl302036x.
[137] D. Metten, G. Froehlicher, S. Berciaud, *2D Materials* **2017**, *4*, 014004.
[138] D. Lloyd, X. Liu, J. W. Christopher, L. Cantley, A. Wadehra, B. L. Kim, B. B. Goldberg, A. K. Swan, J. S. Bunch, *Nano Lett.* **2016**, *16*, 5836.
[139] R. J. Weiss, *Phys. Rev.* **1965**, *140*, A1867.
[140] N. Levy, S. A. Burke, K. L. Meaker, M. Panlasigui, A. Zettl, F. Guinea, A. H. C. Neto, M. F. Crommie, *Science* **2010**, *329*, 544.
[141] M. Neek-Amal, F. M. Peeters, *Phys. Rev. B* **2012**, *85*, 195445.
[142] A. Summerfield, A. Davies, T. S. Cheng, V. V. Korolkov, Y. Cho, C. J. Mellor, C. T. Foxon, A. N. Khlobystov, K. Watanabe, T. Taniguchi, L. Eaves, S. V. Novikov, P. H. Beton, *Scientific Reports* **2016**, *6*, 22440.
[143] O. Lopez-Sanchez, D. Lembke, M. Kayci, A. Radenovic, A. Kis, *Nat. Nanotechnol.* **2013**, *8*, 497.
[144] J.-H. L. G.-H. L. C.-H. Lee, J. Y. Shin, *Nanomaterials* **2016**, *6*, 193.
[145] K. S. Novoselov, A. H. C. Neto, *Phys. Scr.* **2012**, *2012*, 014006.
[146] M. S. Dresselhaus, A. Jorio, M. Hofmann, G. Dresselhaus, R. Saito, *Nano Lett.* **2010**, *10*, 751.
[147] C. Vo-Van, A. Kimouche, A. Reserbat-Plantey, O. Fruchart, P. Bayle-Guillemaud, N. Bendiab, J. Coraux, *Appl. Phys. Lett.* **2011**, *98*, 181903.
[148] Y. Wang, Z. Ni, T. Yu, Z. Shen, *J. Phys. Chem. C* **2008**, 10637.
[149] I. Calizo, W. Bao, F. Miao, C. N. Lau, A. A. Balandin, *Appl. Phys. Lett.* **2007**, *91*, 2.
[150] Z. Han, A. Kimouche, D. Kalita, A. Allain, H. Arjmandi-Tash, A. Reserbat-Plantey, L. Marty, S. Pairis, V. Reita, N. Bendiab, J. Coraux, V. Bouchiat, *Adv. Funct. Mater.* **2014**, *24*, 964.
[151] Q. H. Wang, Z. Jin, K. K. Kim, A. J. Hilmer, G. L. C. Paulus, C.-J. Shih, M.-H. Ham, J. D. Sanchez-Yamagishi, K. Watanabe, T. Taniguchi, J. Kong, P. Jarillo-Herrero, M. S. Strano, *Nat. Chem.* **2012**, *4*, 724.
[152] H. Arjmandi-Tash, *http://www.theses.fr,*. Thesis, Université Grenoble Alpes, **2014**.